

Derivation, Cross-Validation, and Comparison of Analytic Formulas for Electrostatic Deflector Aberrations

Eremey Valetov and Martin Berz

December 30, 2019

Abstract

We derived first and second order analytic aberration formulas in the horizontal transverse plane for an electrostatic deflector specified by the reference orbit radius, the central angle spanning the deflector, and its inhomogeneity coefficients. The derivation was performed using an iterative order-by-order perturbation method in a Frenet–Serret beamline coordinate system. We produced a C program `edabrt` for calculation of the first and second order aberrations using the formulas that we derived.

The electrostatic deflector aberration formulas from Wollnik (1965) disagree with *COSY INFINITY* and the aberration formulas that we derived here, and they also deviate from the first and second order symplecticity conditions. The reason for this discrepancy is that the aberration formulas from Wollnik (1965) consider only motion in the main field of the deflector and do not properly account for fringe field effects, in particular the necessarily occurring change of kinetic energy due to the change in potential. The code *GIOS* uses electrostatic aberration formulas from Wollnik (1965) and exhibits the same discrepancy.

We performed a comparison of first and second order electrostatic deflector aberrations for (1) the analytic formulas derived in this work, (2) differential-algebraic (DA) numerical integration of the equations of motion using the code *COSY INFINITY*, (3) the aberration formulas from Wollnik (1965), (4) aberrations computed using the code *GIOS*, and (5) the aberration formulas from Wollnik (1965) adjusted to account for the occurring change in potential. An electrostatic spherical deflector and an electrostatic cylindrical deflector were used as test cases for this comparison. There is excellent agreement between methods (1), (2), and (5), and these three methods satisfy the first and second order symplecticity conditions.

Keywords: electrostatic deflectors, aberrations, fringe fields, *COSY INFINITY*
Michigan State University, East Lansing, MI 48824, USA

Contents

1	Introduction	2
2	General Considerations	3
3	Order-by-Order Derivation of Aberration Formulas	4
4	Comparison of Derived Aberrations Formulas with <i>COSY INFINITY</i>, <i>GIOS</i>, and Wollnik’s Paper	10
4.1	Electrostatic Spherical Deflector Aberrations	12
4.1.1	Case EDABRT	12
4.1.2	Cases <i>COSY</i> , <i>COSY_CO7</i> , and <i>COSY_CO7_TY0</i>	13
4.1.3	Cases <i>COSY</i> , <i>COSY_CO7</i> , and <i>COSY_CO7_TY0</i> (relativistic ODEs)	13
4.1.4	Case <i>LEGACY1965</i>	14

4.1.5	Case GIOS	15
4.1.6	Case LEGACY1965_Mod	15
4.2	Electrostatic Cylindrical Deflector Aberrations	16
4.2.1	Case EDABRT	16
4.2.2	Cases COSY, COSY_CO7, and COSY_CO7_TY0	16
4.2.3	Cases COSY, COSY_CO7, and COSY_CO7_TY0 (relativistic ODEs)	17
4.2.4	Case LEGACY1965	18
4.2.5	Case GIOS	18
4.2.6	Case LEGACY1965_Mod	19
4.3	Comparison of Particle Tracking Results	19
5	Conclusion	33
6	Electronic Supplementary Material	33
7	Acknowledgment	34
	References	34
A	Derivation of the ODEs of Motion in Beamline Coordinates	36
A.1	Frenet–Serret Coordinate System	36
A.1.1	Basis and Coordinate Transformations	37
A.1.2	Frenet–Serret Theorem	37
A.1.3	Beam Physics Conventions	39
A.1.4	Velocity in the Frenet–Serret Coordinate System	39
A.2	Lagrangian of a Charged Particle	40
A.3	Derivation of the Equations of Motion	40
A.3.1	Result of the Derivation	44
B	Inhomogeneity Coefficients of Electrostatic Spherical and Cylindrical Deflectors	44

1 Introduction

In comparison to homogeneous magnetic dipoles, the use of electrostatic deflectors in particle accelerator beamlines and storage rings has been limited because for realistically achievable fields, the bending power of electrostatic deflectors is significantly lower than for magnetic fields. Electrostatic deflectors generally have nonlinear aberrations of all orders, which must be taken into account to perform accurate modeling and simulations. Recently, there is a renewed interest in electrostatic deflectors, in particular because they are necessary to measure the electrostatic dipole moment (EDM) using a storage ring with the frozen spin (Anastassopoulos et al., 2008) or quasi-frozen spin (Senichev et al., 2015; Valetov, 2017) method. Electrostatic deflectors are also used in spectroscopy for ion beam analysis. In a recent paper (Valetov, Berz, & Makino, in print), we validated the differential-algebraic (DA) transfer map calculation for electrostatic deflectors using the code *COSY INFINITY* (Makino & Berz, 2006) by comparing with calculations of these DA transfer maps in the polar laboratory coordinates, and we found a significant discrepancy with the code *GIOS*, which uses aberration formulas from Wollnik (1965) (“Wollnik’s paper”). The electrostatic deflector transfer maps computed by Valetov et al. (in print) using *COSY INFINITY* satisfy the first and second order symplecticity conditions, while the transfer maps computed using *GIOS* significantly deviate from the second order symplecticity conditions.

Here, we will derive first and second order aberration formulas in the horizontal transverse plane x - a of *COSY INFINITY*’s beamline coordinate system for an electrostatic deflector of reference orbit radius R_0 , central angle α , and electrostatic field $E(x)$ in the midplane defined by first and second order inhomogeneity indices n_1 and n_2 . The derivation will be performed using an iterative order-by-order perturbation method,

resulting in exact, analytic aberration formulas. We will use non-relativistic equations of motion, making our aberration formulas directly comparable with *GIOS* and the aberration formulas from Wollnik’s paper. We will produce a C program named `edabrt` that calculates the first and second order aberrations using our analytic formulas.

We will show that there is excellent agreement between the analytic aberration formulas that we derived and *COSY INFINITY*, and that aberrations computed using both methods satisfy the symplecticity conditions. On the other hand, there is a significant discrepancy with analytic formulas from Wollnik’s paper and the program *GIOS*. Valetov (in this volume) performed an analysis of the derivation of aberration formulas in Wollnik’s paper, showing that the reason for this discrepancy is that Wollnik’s paper considers only motion within the main field and does not have fringe field considerations. Valetov (in this volume) modified the aberration formulas from Wollnik’s paper to account for a hard edge fringe field. This modification results in a full agreement with our aberration formulas and *COSY INFINITY*, which we will demonstrate here.

To cross-validate the derived aberration formulas, we implemented a *COSY INFINITY* program `ESCP010AIEP.FOX` to calculate the first and second order aberrations for electrostatic spherical and cylindrical deflectors using the analytical formulas derived here, *COSY INFINITY*’s built-in elements `ESP` and `ECL`, and analytic formulas from Wollnik’s paper (both original and adjusted for a hard edge fringe field). The program `ESCP010AIEP.FOX` also contains aberrations calculated for these deflectors using the program *GIOS*.

This work validates the computation of aberrations and thus also transfer maps of electrostatic deflectors in *COSY INFINITY* in a complementary way to its validation by Valetov et al. (in print), and it provides first and second order analytic aberration formulas for electrostatic deflectors in the horizontal transverse plane.

2 General Considerations

The code *COSY INFINITY* uses a beamline coordinate system with the phase space coordinates (Berz & Makino, 2017)

$$\begin{aligned} r_1 &= x, & r_2 &= a = p_x/p_0, \\ r_3 &= y, & r_4 &= b = p_y/p_0, \\ r_5 &= l = -(t - t_0)v_0 \frac{\gamma}{1+\gamma}, & r_6 &= \delta_K = \frac{K-K_0}{K}. \end{aligned}$$

Coordinates x and y are the transverse Frenet-Serret position coordinates (see appendix section A.1.3 for the beam physics conventions of the Frenet-Serret formalism), p is the momentum, K is the kinetic energy, v is the velocity, t is the time of flight, and γ is the Lorentz factor. Index 0 refers to the reference particle. The arc length coordinate in *COSY INFINITY* is denoted by s .

COSY INFINITY’s particle optical elements `ESP` and `ECL` compute the transfer map of electrostatic spherical and cylindrical deflectors, respectively. Additionally, *COSY INFINITY*’s inhomogeneous combined-function electrostatic elements `ES` and `EC` calculate the transfer map for electrostatic deflectors with the electrostatic field $E(x)$ in the midplane x - s given by inhomogeneity indices n_j in the expansion

$$E(x) = E_0 \left[1 - \sum_{j=1}^N n_j \left(\frac{x}{R_0} \right)^j \right] + O(x^{N+1}), \quad (1)$$

where R_0 is the reference orbit radius. The expansion order N is $N = 5$ in case of `ES` and an arbitrary natural number in case of `EC`. The electrostatic deflectors are assumed to have the midplane symmetry.

We consider an ensemble of non-relativistic particles of mass m and charge Ze , where e is the elementary charge. The particles are launched with kinetic energy $K_0 = mv_0^2/2$, where v_0 is the reference velocity. We denote the electrostatic potential by φ .

Let h be the curvature of the reference orbit, $\eta = [K_0(1 + \delta_K) - Ze\varphi]/mc^2$ a relativistic measure, $p = mv$ the particle momentum, and

$$\zeta = \frac{p_s}{p_0} = \sqrt{\frac{\eta}{\eta_0} - a^2 - b^2} \quad (2)$$

the scaled longitudinal component of the momentum.

We denote the electric and magnetic rigidities by $\chi_e = pv/Ze$ and $\chi_m = p/Ze$, respectively. We use the convention of the electrostatic potential φ as zero for the reference particle. Hence, $\eta_0 = K_0/mc^2$.

The particle beam is subject to the following non-relativistic ODEs of motion (Makino & Berz, 2015; Valetov, 2017), which we derived for coordinates x , a , y , and b in App. A.

$$\begin{aligned} x' &= a(1+hx)\frac{1}{\zeta}, & a' &= (1+hx)\left(\frac{1}{\zeta}\frac{E_x}{\chi_{e0}} - \frac{B_y}{\chi_{m0}} + b\frac{1}{\zeta}\frac{B_s}{\chi_{m0}}\right) + h\zeta, \\ y' &= b(1+hx)\frac{1}{\zeta}, & b' &= (1+hx)\left(\frac{1}{\zeta}\frac{E_y}{\chi_{e0}} + \frac{B_x}{\chi_{m0}} - a\frac{1}{\zeta}\frac{B_s}{\chi_{m0}}\right), \\ \delta'_K &= 0, & l' &= -\frac{1}{2}\left[(1+hx)\frac{1}{\zeta} - 1\right]. \end{aligned}$$

These non-relativistic ODEs of motion were used by Valetov et al. (in print) for a test case calculation of *COSY INFINITY*'s electrostatic deflector elements ESP and ECL. Valetov et al. (in print) ascertained that the resulting transfer maps agree with the results of integrating trivial non-relativistic ODEs of motion in a laboratory coordinate system and, in case of an electrostatic spherical deflector, analytic Kepler theory solutions.

For any $f, g \in C^n(\mathbb{R}^k)$, where n is the order and k is the number of variables, will use the DA equivalence relation $f =_n g$ to denote that $f(0) = g(0)$ and all partial derivatives of f and g agree at 0 up to order n . See Berz (1999) for detailed information on DA algebra.

Because of the choice of variables in *COSY INFINITY*'s beamline coordinate system, the coordinates $(x, a, y, b, \delta_K, l)$ are invariant in a traversal through a hard edge fringe field. On the other hand, in the coordinate system used in Wollnik's paper, the momentum coordinates need to be transformed to account for the diffractive effects of the change in potential in a fringe field including the hard edge fringe field model (Valetov, in this volume).

3 Order-by-Order Derivation of Aberration Formulas

For an electrostatic deflector with reference orbit curvature $h = R_0^{-1}$ and inhomogeneity indices n_1, n_2 as per eq. 1, the second order DA representation of the non-relativistic ODE of x - a motion in the electrostatic deflector is

$$\frac{d}{ds} \begin{pmatrix} x \\ a \end{pmatrix} =_2 \frac{1}{\zeta} \begin{pmatrix} a(1+hx) \\ (1+hx)E_x/\chi_{e0} + h\zeta^2 \end{pmatrix}, \quad (3)$$

where χ_{e0} is the reference electric rigidity $\chi_{e0} = mv_0^2/Ze$, the E_x component of the electrostatic field is

$$E_x =_2 E_x(x) =_2 E_0 \left(1 - \sum_{j=1}^2 n_j h^j x^j \right) \quad (4)$$

in the midplane,

$$\zeta = \sqrt{\frac{\eta}{\eta_0} - a^2} \quad (5)$$

expresses ζ from eq. 2 in the midplane, and

$$\eta = \frac{1}{mc^2} (K_0(1 + \delta_K) - Ze\varphi). \quad (6)$$

We note that the inhomogeneity indices (n_1, n_2) are $(2, -3)$ for an electrostatic spherical deflector and $(1, -1)$ for an electrostatic cylindrical deflector (see App. B or Berz and Makino, 2017).

By Newton's second law, zero radial acceleration at the reference orbit requires

$$ZeE_0 + \frac{mv_0^2}{R_0} = 0, \quad (7)$$

which we rewrite as

$$E_0 = -h\chi_{e0}. \quad (8)$$

To obtain the electrostatic potential in the midplane, we integrate the electrostatic field:

$$\begin{aligned} \varphi(x) &= {}_3 \varphi(x, y)|_{y=0} = {}_3 -\partial_x^{-1} E_x(x) = {}_3 \\ &= {}_3 -E_0 x + \frac{1}{2} E_0 h n_1 x^2 + \frac{1}{3} E_0 h^2 n_2 x^3. \end{aligned} \quad (9)$$

We have for ζ , considering eqns. 9 and 8,

$$\begin{aligned} \zeta &= {}_2 \sqrt{\frac{\eta}{\eta_0} - a^2} = {}_2 \\ &= {}_2 \sqrt{1 + \delta_K - \frac{2Ze\varphi}{mv_0^2} - a^2} = {}_2 \\ &= {}_2 \left(1 + \delta_K - a^2 - \frac{2}{\chi_{e0}} \left(-E_0 x + \frac{1}{2} E_0 h n_1 x^2 + \frac{1}{3} E_0 h^2 n_2 x^3 \right) \right)^{\frac{1}{2}} = {}_2 \\ &= {}_2 1 - \frac{a^2}{2} + \frac{\delta_K}{2} - \frac{\delta_K^2}{8} + h \left(\frac{1}{2} \delta_K - 1 \right) x + \frac{1}{2} h^2 (n_1 - 1) x^2, \end{aligned} \quad (10)$$

from where we also obtain

$$\frac{1}{\zeta} = {}_2 1 + \frac{a^2}{2} - \frac{\delta_K}{2} + \frac{3}{8} \delta_K^2 + h \left(1 - \frac{3}{2} \delta_K \right) x + \frac{1}{2} h^2 (3 - n_1) x^2.$$

Applying this to eq. 3, we have

$$\frac{d}{ds} \begin{pmatrix} x \\ a \end{pmatrix} = {}_2 \begin{pmatrix} a + 2ahx \\ h^2 (n_1 - 3) x + h^3 (3n_1 + n_2 - 3) x^2 - ha^2 \end{pmatrix}, \quad (11)$$

where we kept only the x - a terms.

Following Berz, Makino, and Wan (2014), performing a Taylor expansion of the right-hand side, we rewrite the ODE of motion

$$\frac{d}{ds} \vec{r} = \vec{f}(\vec{r}, s) \quad (12)$$

as

$$\frac{d}{ds} \vec{r} = \hat{M}(s) \vec{r} + \sum_{j=2}^{+\infty} \vec{N}_j(\vec{r}, s), \quad (13)$$

where $\hat{M}(s)$ is a square matrix and $\vec{N}_j(\vec{r}, s)$ are polynomials of exact order j in the beamline coordinates, coefficients of which generally may depend on s . In this one-dimensional derivation,

$$\vec{r} = \begin{pmatrix} x \\ a \end{pmatrix}. \quad (14)$$

Comparing eqns. 11 and 13, we find that

$$\hat{M}(s) = \begin{pmatrix} 0 & 1 \\ -3h^2 + h^2 n_1 & 0 \end{pmatrix} \quad (15)$$

and

$$\vec{N}_2(\vec{r}, s) = \begin{pmatrix} 2ahx \\ h^3 (3n_1 + n_2 - 3) x^2 - ha^2 \end{pmatrix}. \quad (16)$$

The main field of the electrostatic deflector is s -independent, which is why $\hat{M}(s)$ and $\vec{N}_2(\vec{r}, s)$ do not depend on s , and we will omit their argument s from here on forward.

First, we solve the equation

$$\frac{d}{ds}\vec{r} = \hat{M} \cdot \vec{r}, \quad (17)$$

which represents a linearization of the ODE of motion.

Because \hat{M} in eq. 17 is s -independent, its solution can be found as (Grimshaw, 1990; Teschl, 2012)

$$\vec{r}_f = \vec{r}(s) = \hat{L}(s) \vec{r}_i = \exp(\hat{M}s) \vec{r}_i, \quad (18)$$

where \vec{r}_i are the initial coordinates $\vec{r}_i = \vec{r}(0)$, \vec{r}_f are the final coordinates $\vec{r}_f = \vec{r}(s)$, and $\exp(\hat{M}s)$ is the matrix exponential

$$\exp(\hat{M}s) = \sum_{j=0}^{+\infty} \frac{1}{j!} \hat{M}^j s^j. \quad (19)$$

Indeed, taking the Laplace transform \mathcal{L} of eq. 17 yields (Dorf & Bishop, 2017)

$$\mathcal{L}\left(\frac{d}{ds}\vec{r}(s) - \hat{M} \cdot \vec{r}(s)\right) = -\vec{r}(0) + (\tilde{s}\hat{I} - \hat{M})\vec{R}(\tilde{s}) = 0,$$

from where we have

$$\vec{R}(\tilde{s}) = (\tilde{s}\hat{I} - \hat{M})^{-1} \vec{r}(0), \quad (20)$$

where \tilde{s} is the complex frequency parameter, \hat{I} is the unit matrix, and $\vec{R}(\tilde{s}) = \mathcal{L}(\vec{r}(s))$. The operator

$$\Phi(\hat{M}) = (\tilde{s}\hat{I} - \hat{M})^{-1} \quad (21)$$

is called the resolvent of \hat{M} (Hunter & Nachtergaele, 2001). We note that

$$\begin{aligned} \mathcal{L}^{-1}\left[(\tilde{s}\hat{I} - \hat{M})^{-1}\right] &= \mathcal{L}^{-1}\left[\sum_{j=0}^{+\infty} \hat{M}^j \tilde{s}^{-j-1}\right] = \\ &= \sum_{j=0}^{+\infty} \frac{1}{j!} \hat{M}^j s^j = \exp(\hat{M}s). \end{aligned} \quad (22)$$

Conversely, the matrix exponential in eq. 19 can be computed using the inverse Laplace transform \mathcal{L}^{-1} as (Dorf & Bishop, 2017)

$$\exp(\hat{M}s) = \mathcal{L}^{-1}\left[(\tilde{s}\hat{I} - \hat{M})^{-1}\right]. \quad (23)$$

We calculate the $\hat{L}(s)$ in eq. 18 using eq. 23:

$$\begin{aligned} \hat{L}(s) &= \exp(\hat{M}s) = \\ &= \mathcal{L}^{-1}\left[(\tilde{s}\hat{I} - \hat{M})^{-1}\right] = \\ &= \mathcal{L}^{-1}\left[\left(\tilde{s}\hat{I} - \begin{pmatrix} 0 & 1 \\ -3h^2 + h^2n_1 & 0 \end{pmatrix}\right)^{-1}\right] = \\ &= \mathcal{L}^{-1}\left[\frac{1}{3h^2 - h^2n_1 + \tilde{s}^2} \begin{pmatrix} \tilde{s} & -1 \\ 3h^2 - h^2n_1 & \tilde{s} \end{pmatrix}\right] = \\ &= \begin{pmatrix} \cos(h\sqrt{3-n_1}s) & \sin(h\sqrt{3-n_1}s)/(h\sqrt{3-n_1}) \\ -h\sqrt{3-n_1}\sin(h\sqrt{3-n_1}s) & \cos(h\sqrt{3-n_1}s) \end{pmatrix}. \end{aligned} \quad (24)$$

The Taylor expansion of $\vec{r}(s)$, considering the solution $\vec{r}(s) = \hat{L}(s) \vec{r}_i$ of the linearized problem, is

$$\vec{r}(s) = \hat{L}(s) \vec{r}_i + \sum_{j=2}^{+\infty} \vec{R}_j(s, \vec{r}_i), \quad (25)$$

where \vec{R}_j is a polynomial of exact order j in the initial conditions, with coefficients as functions of s .

Inserting the Taylor expansion of $\vec{r}(s)$ from eq. 25 into the ODE as written in eq. 13, we obtain

$$\begin{aligned} \frac{d}{ds} \vec{r}(s) &= \left(\frac{d}{ds} \hat{L}(s) \right) \vec{r}_i + \sum_{j=2}^{+\infty} \frac{d}{ds} \vec{R}_j(s, \vec{r}_i) = \\ &= \hat{M} \hat{L}(s) \vec{r}_i + \hat{M} \sum_{j=2}^{+\infty} \vec{R}_j(s, \vec{r}_i) + \sum_{j=2}^{+\infty} \vec{Q}_j(s, \hat{L}, \vec{R}_j), \end{aligned} \quad (26)$$

where

$$\vec{Q}_j(s, \hat{L}, \vec{R}_j) = \vec{N}_j(\vec{r}(s, \hat{L}, \vec{R}_j)) \quad (27)$$

is a polynomial of exact order j in \vec{r} .

The linear part of eq. 26 gives

$$\frac{d}{ds} \hat{L}(s) = \hat{M} \hat{L}(s), \quad (28)$$

and its parts of orders $j \geq 2$ give

$$\frac{d}{ds} \vec{R}_j(s, \vec{r}_i) = \hat{M} \vec{R}_j(s, \vec{r}_i) + \vec{Q}_j(s, \hat{L}, \vec{R}_j). \quad (29)$$

At $s = 0$, $\vec{r}(s)$ is the initial condition \vec{r}_i . By eq. 25, this yields $\hat{L}(0) = \hat{I}$ and $\vec{R}_j(0, \vec{r}_i) = 0$ for all $j \geq 2$.

The polynomial \vec{Q}_2 will be useful in the calculations below. To find \vec{Q}_2 , we insert the linear solution specified by eqns. 18 and 24 into the ODE expansion from eq. 11, obtaining

$$\begin{aligned} \frac{d}{ds} x_f &= a_f + 2a_f h x_f = \\ &= (\cos(\xi s) a_i - \xi \sin(\xi s) x_i) [1 + 2h (\cos(\xi s) x_i + \xi^{-1} \sin(\xi s) a_i)] \end{aligned} \quad (30)$$

and

$$\begin{aligned} \frac{d}{ds} a_f &= h^2 (n_1 - 3) x_f + h^3 (3n_1 + n_2 - 3) x_f^2 - h a_f^2 = \\ &= h^2 (\cos(\xi s) x_i + \xi^{-1} \sin(\xi s) a_i) [n_1 - 3 + \\ &+ h (3n_1 + n_2 - 3) (\cos(\xi s) x_i + \xi^{-1} \sin(\xi s) a_i)] - \\ &- h (\cos(\xi s) a_i - \xi \sin(\xi s) x_i)^2, \end{aligned} \quad (31)$$

where $\xi = h\sqrt{3 - n_1}$.

Next, we extract the second order part \vec{Q}_2 from the right-hand sides of eqns. 30 and 31:

$$\begin{aligned} \vec{Q}_2 &= \begin{pmatrix} Q_{2x} \\ Q_{2a} \end{pmatrix} = \\ &= \begin{pmatrix} -h\xi \sin(2\xi s) & \frac{1}{2}h^3(4n_1 + n_2 - 6 + (2n_1 + n_2)\cos(2\xi s)) \\ 2h \cos(2\xi s) & h^3 \xi^{-1} (2n_1 + n_2) \sin(2\xi s) \\ h\xi^{-1} \sin(2\xi s) & \frac{1}{2}h^3 \xi^{-2} (4n_1 + n_2 - 6 - (2n_1 + n_2)\cos(2\xi s)) \end{pmatrix}^T \begin{pmatrix} x_i^2 \\ x_i a_i \\ a_i^2 \end{pmatrix}. \end{aligned} \quad (32)$$

The solution $\vec{r}(s) = \hat{L}(s) \vec{r}_i$ of the linearized problem is the homogeneous solution of eq. 26. To obtain its second order inhomogeneous solution, we perform the ansatz

$$\vec{R}_2(s) = \hat{L}(s) \vec{T}(s). \quad (33)$$

Inserting eq. 33 into eq. 29 with $j = 2$, considering eq. 28, we have

$$\begin{aligned}\frac{d}{ds}\vec{R}_2(s) &= \left(\frac{d}{ds}\hat{L}(s)\right)\vec{T}(s) + \hat{L}(s)\left(\frac{d}{ds}\vec{T}(s)\right) = \\ &= \hat{M}\hat{L}(s)\vec{T}(s) + \hat{L}(s)\left(\frac{d}{ds}\vec{T}(s)\right) = \\ &= \hat{M}\hat{L}(s)\vec{T}(s) + \vec{Q}_2(s),\end{aligned}\tag{34}$$

which yields

$$\hat{L}(s) \cdot \frac{d}{ds}\vec{T}(s) = \vec{Q}_2(s).\tag{35}$$

Solving eq. 35 for $\vec{T}(s)$, we obtain

$$\vec{T}(s) = \begin{pmatrix} T_x \\ T_a \end{pmatrix} = \int_0^s \hat{L}^{-1}\vec{Q}_2 ds,\tag{36}$$

where, considering that $\det(\hat{L}(s)) = 1$,

$$\hat{L}^{-1}(s) = \begin{pmatrix} \cos(\xi s) & -\xi^{-1}\sin(\xi s) \\ \xi \sin(\xi s) & \cos(\xi s) \end{pmatrix}.$$

The integral in eq. 36 is called the aberration integral, and its integrand is called the driving term (Berz et al., 2014).

We obtain for elements T_x and T_a of vector $\vec{T}(s)$:

$$\begin{aligned}T_x &= \int_0^s \left(\hat{L}_{11}^{-1}Q_{2x} + \hat{L}_{12}^{-1}Q_{2a} \right) ds = \\ &= \int_0^s \left[\cos(\xi s) (-h\xi \sin(2\xi s) x_i^2 + 2h \cos(2\xi s) x_i a_i + h\xi^{-1} \sin(2\xi s) a_i^2) - \right. \\ &\quad \left. -\xi^{-1} \sin(\xi s) \left(h^3 (2n_1 + n_2) \left(\frac{1}{2} \cos(2\xi s) (x_i^2 - \xi^{-2} a_i^2) + \xi^{-1} \sin(2\xi s) x_i a_i \right) + \right. \right. \\ &\quad \left. \left. + \frac{1}{2} h^3 (4n_1 + n_2 - 6) (x_i^2 + \xi^{-2} a_i^2) \right) \right] ds\end{aligned}\tag{37}$$

and

$$\begin{aligned}T_a &= \int_0^s \left(\hat{L}_{21}^{-1}Q_{2x} + \hat{L}_{22}^{-1}Q_{2a} \right) ds = \\ &= \int_0^s \left[\xi \sin(\xi s) (-h\xi \sin(2\xi s) x_i^2 + 2h \cos(2\xi s) x_i a_i + h\xi^{-1} \sin(2\xi s) a_i^2) + \right. \\ &\quad \left. + \cos(\xi s) \left(h^3 (2n_1 + n_2) \left(\frac{1}{2} \cos(2\xi s) (x_i^2 - \xi^{-2} a_i^2) + \xi^{-1} \sin(2\xi s) x_i a_i \right) + \right. \right. \\ &\quad \left. \left. + \frac{1}{2} h^3 (4n_1 + n_2 - 6) (x_i^2 + \xi^{-2} a_i^2) \right) \right] ds.\end{aligned}\tag{38}$$

We collect the x_i^2 , $x_i a_i$, and a_i^2 terms, and we carry out the integration:

$$\begin{aligned}T_x &= \int_0^s \begin{pmatrix} -\frac{1}{2}h^3\xi^{-1}(2n_1 + n_2 + (6 + n_2)\cos(2\xi s))\sin(\xi s) \\ -h^3\xi^{-2}(2n_1 + n_2 - (6 + n_2)\cos(2\xi s))\cos(\xi s) \\ -\frac{1}{2}h^3\xi^{-3}(6n_1 + n_2 - 12 - (6 + n_2)\cos(2\xi s))\sin(\xi s) \end{pmatrix}^T ds \cdot \begin{pmatrix} x_i^2 \\ x_i a_i \\ a_i^2 \end{pmatrix} = \\ &= \begin{pmatrix} -\frac{1}{3}h^3\xi^{-2}(3(2n_1 + n_2) + (6 + n_2)(2\cos(\xi s) + \cos(2\xi s)))\sin^2(\frac{1}{2}\xi s) \\ -\frac{1}{3}h^3\xi^{-3}(6n_1 + n_2 - 12 - (6 + n_2)\cos(2\xi s))\sin(\xi s) \\ \frac{1}{3}h^3\xi^{-4}(3(12 - 6n_1 - n_2) + (6 + n_2)(2\cos(\xi s) + \cos(2\xi s)))\sin^2(\frac{1}{2}\xi s) \end{pmatrix}^T \begin{pmatrix} x_i^2 \\ x_i a_i \\ a_i^2 \end{pmatrix}\end{aligned}\tag{39}$$

and

$$\begin{aligned}
T_a &= \int_0^s \begin{pmatrix} \frac{1}{2}h^3(6n_1+n_2-12+(6+n_2)\cos(2\xi s))\cos(\xi s) \\ h^3\xi^{-1}(2n_1+n_2+(6+n_2)\cos(2\xi s))\sin(\xi s) \\ \frac{1}{2}h^3\xi^{-2}(2n_1+n_2-(6+n_2)\cos(2\xi s))\cos(\xi s) \end{pmatrix}^T ds \cdot \begin{pmatrix} x_i^2 \\ x_i a_i \\ a_i^2 \end{pmatrix} = \\
&= \begin{pmatrix} \frac{1}{6}h^3\xi^{-1}(18n_1+5n_2-24+(6+n_2)\cos(2\xi s))\sin(\xi s) \\ \frac{2}{3}h^3\xi^{-2}(3(2n_1+n_2)+(6+n_2)(2\cos(\xi s)+\cos(2\xi s)))\sin^2(\frac{1}{2}\xi s) \\ -\frac{1}{6}h^3\xi^{-3}(12-6n_1-n_2+(6+n_2)\cos(2\xi s))\sin(\xi s) \end{pmatrix}^T \begin{pmatrix} x_i^2 \\ x_i a_i \\ a_i^2 \end{pmatrix}. \tag{40}
\end{aligned}$$

Using the notation of Wollnik and Berz (1985), we will consider the coefficients

$$(z_i|z_{j_1}\cdots z_{j_n}) = \left(\frac{\partial^n (\mathcal{M}(z))_i}{\partial z_{j_1}\cdots\partial z_{j_n}} \right)_{z=0} \tag{41}$$

of the i -th component of the respective transfer map $\mathcal{M}(z)$, where z is a coordinate vector $z = (z_1, \dots, z_{2m})$ and $2m$ is the number of phase space coordinates. Aberration coefficients can be expressed in terms of the respective partial derivatives $(z_i|z_{j_1}\cdots z_{j_n})$ as

$$\frac{1}{j_1!\cdots j_n!} (z_i|z_{j_1}\cdots z_{j_n}). \tag{42}$$

In the following, we will use coefficients $(z_i|z_{j_1}\cdots z_{j_n})$ to describe the aberrations.

The first order coefficients $(z_i|z_{j_1})$ are the elements of the linear part $\hat{L}(s)$ of the transfer map. Noting that $\vec{R}_2(s)$ is the second order part of the transfer map, the second order coefficients $(z_i|z_{j_1}z_{j_2})$ are

$$(z_i|z_{j_1}z_{j_2}) = j_1!j_2! [(z_{j_1})_i (z_{j_2})_i] (\vec{R}_2(s))_i, \tag{43}$$

where $[z]f$ denotes the coefficient of z in f (Graham, Knuth, & Patashnik, 1994).

From eq. 24, we extract the first order aberrations:

$$(x|x) = \hat{L}_{11} = \cos(\xi s), \tag{44a}$$

$$(x|a) = \hat{L}_{12} = \xi^{-1} \sin(\xi s), \tag{44b}$$

$$(a|x) = \hat{L}_{21} = -\xi \sin(\xi s), \tag{44c}$$

$$(a|a) = \hat{L}_{22} = \cos(\xi s). \tag{44d}$$

We obtain (Berz et al., 2014) the second order aberrations using eqns. 24, 33, 39, 40, and 43:

$$\begin{aligned}
\frac{1}{2}(x|xx) &= [x_i^2] \left(\hat{L}_{11}T_x + \hat{L}_{12}T_a \right) = \\
&= -\frac{1}{3}h^3\xi^{-2} (3(2n_1+n_2) + (6+n_2)(2\cos(\xi s) + \cos(2\xi s))) \sin^2\left(\frac{1}{2}\xi s\right) \cos(\xi s) + \\
&+ \frac{1}{6}h^3\xi^{-2} (18n_1+5n_2-24+(6+n_2)\cos(2\xi s)) \sin^2(\xi s) = \\
&= \frac{2}{3}h^3\xi^{-2} (9n_1+2n_2-15+(6n_1+n_2-12)\cos(\xi s)) \sin^2\left(\frac{1}{2}\xi s\right), \tag{45a}
\end{aligned}$$

$$\begin{aligned}
(x|xa) &= [x_i a_i] \left(\hat{L}_{11}T_x + \hat{L}_{12}T_a \right) = \\
&= -\frac{1}{6}h^3\xi^{-3} (6n_1+n_2-12-(6+n_2)\cos(2\xi s)) \sin(2\xi s) + \\
&+ \frac{2}{3}h^3\xi^{-3} (3(2n_1+n_2) + (6+n_2)(2\cos(\xi s) + \cos(2\xi s))) \sin^2\left(\frac{1}{2}\xi s\right) \sin(\xi s) = \\
&= \frac{2}{3}h^3\xi^{-3} (3n_1+n_2-3-(6n_1+n_2-12)\cos(\xi s)) \sin(\xi s), \tag{45b}
\end{aligned}$$

$$\begin{aligned}
\frac{1}{2}(x|aa) &= [a_i^2] \left(\hat{L}_{11}T_x + \hat{L}_{12}T_a \right) = \\
&= \frac{1}{3}h^3\xi^{-4} \left(3(12 - 6n_1 - n_2) + (6 + n_2)(2\cos(\xi s) + \cos(2\xi s)) \right) \sin^2\left(\frac{1}{2}\xi s\right) \cos(\xi s) - \\
&- \frac{1}{6}h^3\xi^{-4} (12 - 6n_1 - n_2 + (6 + n_2)\cos(2\xi s)) \sin^2(\xi s) = \\
&= \frac{2}{3}h^3\xi^{-4} (3n_1 + n_2 - 3 - (6n_1 + n_2 - 12)\cos(\xi s)) \sin^2\left(\frac{1}{2}\xi s\right),
\end{aligned} \tag{45c}$$

$$\begin{aligned}
\frac{1}{2}(a|xx) &= [x_i^2] \left(\hat{L}_{21}T_x + \hat{L}_{22}T_a \right) = \\
&= \frac{1}{3}h^3\xi^{-1} \left(3(2n_1 + n_2) + (6 + n_2)(2\cos(\xi s) + \cos(2\xi s)) \right) \sin^2\left(\frac{1}{2}\xi s\right) \sin(\xi s) + \\
&+ \frac{1}{12}h^3\xi^{-1} (18n_1 + 5n_2 - 24 + (6 + n_2)\cos(2\xi s)) \sin(2\xi s) = \\
&= \frac{1}{3}h^3\xi^{-1} (3n_1 + n_2 - 3) (\sin(\xi s) + \sin(2\xi s)),
\end{aligned} \tag{45d}$$

$$\begin{aligned}
(a|xa) &= [x_i a_i] \left(\hat{L}_{21}T_x + \hat{L}_{22}T_a \right) = \\
&= \frac{1}{3}h^3\xi^{-2} (6n_1 + n_2 - 12 - (6 + n_2)\cos(2\xi s)) \sin^2(\xi s) + \\
&+ \frac{2}{3}h^3\xi^{-2} \left(3(2n_1 + n_2) + (6 + n_2)(2\cos(\xi s) + \cos(2\xi s)) \right) \sin^2\left(\frac{1}{2}\xi s\right) \cos(\xi s) = \\
&= \frac{2}{3}h^3\xi^{-2} (3n_1 + n_2 - 3) (\cos(\xi s) - \cos(2\xi s)),
\end{aligned} \tag{45e}$$

$$\begin{aligned}
\frac{1}{2}(a|aa) &= [a_i^2] \left(\hat{L}_{21}T_x + \hat{L}_{22}T_a \right) = \\
&= -\frac{1}{3}h^3\xi^{-3} \left(3(12 - 6n_1 - n_2) + (6 + n_2)(2\cos(\xi s) + \cos(2\xi s)) \right) \sin^2\left(\frac{1}{2}\xi s\right) \sin(\xi s) - \\
&- \frac{1}{12}h^3\xi^{-3} (12 - 6n_1 - n_2 + (6 + n_2)\cos(2\xi s)) \sin(2\xi s) = \\
&= \frac{1}{3}h^3\xi^{-3} (9n_1 + 2n_2 - 15 - 2(3n_1 + n_2 - 3)\cos(\xi s)) \sin(\xi s),
\end{aligned} \tag{45f}$$

where $\xi = h\sqrt{3-n_1}$ and $[z]f$ denotes the coefficient of z in f . The arc length is $s = \alpha h^{-1} = \alpha R_0$, where α is the central angle and R_0 is the reference orbit radius specifying the deflector geometry.

The aberration formulas in eqns. 44 and 45 remain valid for $n_1 > 3$, entailing trivial computations with complex numbers or an equivalent restatement in terms of hyperbolic trigonometric functions \sinh and \cosh . The same derivation method as used above is applicable to the special case $n_1 = 3$, with the difference that $n_1 = 3$ is assumed at the beginning of the derivation. Without proof, we will state the analytic aberration formulas for the special case $n_1 = 3$: $(x|x) = 1$, $(x|a) = s$, $(x|xx)/2 = h^3(6+n_2)s^2/2$, $(x|xa) = 2hs + h^3(6+n_2)s^3/3$, $(x|aa)/2 = hs^2(6+h^2(6+n_2)s^2)/12$, $(a|x) = 0$, $(a|a) = 1$, $(a|xx)/2 = h^3(6+n_2)s$, $(a|xa) = h^3(6+n_2)s^2$, and $(a|aa)/2 = hs(h^2(6+n_2)s^2 - 3)/3$.

4 Comparison of Derived Aberrations Formulas with *COSY IN-FINITY*, *GIOS*, and Wollnik's Paper

We composed a C program called `edabrt` that calculates the first and second order aberrations of an electrostatic deflector in the x - a plane using the analytical formulas from eqns. 44–45. The program is provided as supplementary electronic material.

We also implemented a *COSY INFINITY* program `ESCP010AIEP.FOX` to compute the aberrations for all of the following cases, and this section compares the resulting aberrations.

Case EDABRT analytic formulas in eqns. 44–45 derived by us in Sec. 3;

Case COSY *COSY INFINITY*'s built-in electrostatic spherical deflector `ESP` and cylindrical deflector `ECL` elements with numerical DA calculations and computation order 2;

Case LEGACY1965 analytic formulas from Wollnik's paper (see eqns. 31 and 42 of Valetov, in this volume);

Case GIOS the `ES` command sequence in the code *GIOS* without specification of fringe field integrals, which calculates transfer maps of electrostatic deflectors based on analytic formulas from Wollnik's paper;

Case LEGACY1965_Mod analytic formulas from Wollnik's paper, modified by Valetov (in this volume) to account for a hard edge fringe field (see eqns. 31 and 56 of Valetov, in this volume);

Case COSY_CO7 *COSY INFINITY*'s built-in electrostatic spherical deflector `ESP` and cylindrical deflector `ECL` elements with numerical DA calculations and computation order 7; and

Case COSY_CO7_TY0 *COSY INFINITY*'s built-in electrostatic spherical deflector `ESP` and cylindrical deflector `ECL` elements with numerical DA calculations, computation order 7, and Extended Poincaré (EXPO)¹ symplectification.

In all these cases, the deflectors are specified by the reference orbit radius $R_0 = 1$ m and central angle $\alpha = 45^\circ$. We remark that the applicability of the compared methods is not limited to electrostatic spherical and cylindrical deflectors; any inhomogeneity indices n_1 and n_2 (or c and \bar{c} in the notation of Wollnik's paper) can be used.

Non-relativistic equations of motion were used in *COSY INFINITY* for commensurability with the non-relativistic aberration formulas in eqns. 44–45, Wollnik's paper, and *GIOS*. For *COSY INFINITY*'s built-in elements, the particle beam was defined by kinetic energy 10^{-7} MeV, mass 1 amu, and charge $1e$; however, as eqns. 44–45 show, these settings have no effect on the aberrations as long as the reference orbit radius is kept the same by adjusting the voltages of the inner and outer shells of the electrostatic deflector (with non-relativistic ODEs of motion). In *COSY INFINITY*, aberrations are the respective elements of the DA transfer map, which is calculated by performing numerical DA integration of the equations of motion.

We provide the program `ESCP010AIEP.FOX` as supplementary electronic material, with the difference from the version used by us here being that it uses relativistic equations of motion with the non-relativistic kinetic energy 10^{-7} MeV for Cases `COSY`, `COSY_CO7`, and `COSY_CO7_TY0`. This is because the standard distribution of *COSY INFINITY* operates with relativistic equations of motion, whereas we used a non-relativistic version of *COSY INFINITY*'s beam physics module `COSY.FOX` in this research. Accordingly, for reference purposes, we list the aberrations produced with relativistic equations of motion in Subsecs. 4.1.3 and 4.2.3.

The default fringe field mode `FR0` was used in *COSY INFINITY*, where no fringe field calculations are performed, which amounts to a hard edge fringe field model for all particle optical elements because of the choice of variables in *COSY INFINITY*'s beamline coordinate system. In *GIOS* calculations, we also used the default fringe field mode where no fringe field calculations are performed; however, *GIOS* uses the coordinate system of Wollnik's paper, for which Valetov (in this volume) demonstrated that not scaling electrostatic deflector aberrations for the hard edge fringe field results in them being valid only for the main field.

The Jacobian $M = \text{Jac}(\mathcal{M})$ of the transfer map \mathcal{M} of any Hamiltonian system satisfies (Berz, 1999) the symplecticity condition $M \cdot \hat{J} \cdot M^T = \hat{J}$, where

$$\hat{J} = \begin{pmatrix} 0 & I_m \\ -I_m & 0 \end{pmatrix}, \quad (46)$$

¹The EXPO generating function provides an optimal symplectification by minimizing Hofer's metric, which is an "essentially unique intrinsic bi-invariant Finsler metric for compactly supported Hamiltonian symplectic maps" (Erdélyi & Berz, 2001).

I_m is an $m \times m$ identity matrix, m is the phase space dimension, and the canonical position (q_1, \dots, q_m) and canonical momentum (p_1, \dots, p_m) coordinates are ordered as $z = (q_1, \dots, q_m, p_1, \dots, p_m)$. For a transfer map Jacobian of x - a motion, the symplecticity condition can be rewritten as $\det(M) = 1$.

In each aberrations calculation case, we computed deviations (Berz, 1999; Wollnik & Berz, 1985)

$$\begin{aligned} g_1 &= (x|x)(a|a) - (a|x)(x|a) - 1, \\ g_2 &= (x|x)(a|xa) - (a|x)(x|xa) + (x|xx)(a|a) - (a|xx)(x|a), \\ g_3 &= (x|x)(a|aa) - (a|x)(x|aa) + (x|xa)(a|a) - (a|xa)(x|a) \end{aligned} \quad (47)$$

from the conditions of symplecticity $g_1 = 0$, $g_2 = 0$, and $g_3 = 0$. We also found that the analytic aberration formulas in Cases EDABRT and LEGACY1965_Mod analytically satisfy these conditions of symplecticity.

We define deviations g_K and g_P from energy and momentum conservation as

$$g_K = \frac{2m}{p_0^2} \Delta K, \quad g_P = \frac{1}{p_0} \Delta P, \quad (48)$$

where Δ refers to the difference between the exit edge and entrance edge values. For motion in the horizontal transverse plane x - a , we have

$$\begin{aligned} g_K &= \Delta (\zeta^2 + a^2) = \\ &= \Delta \left(\frac{\eta}{\eta_0} \right) = \Delta (1 + \delta_K) \end{aligned} \quad (49)$$

and

$$\begin{aligned} g_P &= \Delta \left(\sqrt{\zeta^2 + a^2} \right) = \\ &= \Delta \left(\sqrt{\frac{\eta}{\eta_0}} \right) = \Delta \left(\sqrt{1 + \delta_K} \right). \end{aligned} \quad (50)$$

The deviations from energy and momentum conservation are expressed in terms of the longitudinal coordinate δ_K and not the horizontal transverse coordinates (x, a) , and these deviations are zero in case of purely horizontal transverse motion, where $\delta_K = 0$.

Valetov et al. (in print) list second order transfer maps for the same electrostatic spherical and cylindrical deflectors, computed in polar laboratory coordinates (1) by integration of the ODEs of motion using a 4th order Runge–Kutta integrator for the electrostatic spherical and cylindrical deflectors and (2) by computing the Kepler theory transition matrix with elements as Lagrange coefficients for the electrostatic spherical deflector. There is excellent agreement between transfer maps computed in polar laboratory coordinates, transfer maps (elements of which are aberrations) computed using *COSY INFINITY*, and analytic aberration formulas from eqns. 44–45 for the electrostatic deflectors.

4.1 Electrostatic Spherical Deflector Aberrations

4.1.1 Case EDABRT

The first and second order aberrations of the electrostatic spherical deflector calculated using the analytic formulas of eqns. 44–45 are as follows.

X:				
I	COEFFICIENT	ORDER	EXPONENTS	
1	0.7071067811865476	1	1	0
2	0.7071067811865475	1	0	1
3	-.5000000000000001	2	2	0
4	1.0000000000000000	2	1	1
5	0.2071067811865476	2	0	2

A:

I	COEFFICIENT	ORDER	EXPONENTS
1	-.7071067811865475	1	1 0
2	0.7071067811865476	1	0 1
3	-.7071067811865475	2	0 2

The deviations g_1 , g_2 , and g_3 from the conditions of symplecticity listed in eq. 47 in this case were

$$\begin{aligned}
g_1 &= 0.0000000000000000, \\
g_2 &= -2.220446049250313 \times 10^{-16}, \\
g_3 &= 1.110223024625157 \times 10^{-16}.
\end{aligned}
\tag{51}$$

4.1.2 Cases COSY, COSY_CO7, and COSY_CO7_TY0

The aberrations of *COSY INFINITY*'s built-in electrostatic spherical deflector element ESP to order 3 calculated with non-relativistic equations of motion are as follows.

X:

I	COEFFICIENT	ORDER	EXPONENTS
1	0.7071067811865475	1	1 0
2	0.7071067811865475	1	0 1
3	-.4999999999999999	2	2 0
4	1.0000000000000000	2	1 1
5	0.2071067811865475	2	0 2
6	-.3535533905932738	3	3 0
7	0.6066017177982123E-01	3	1 2
8	0.2928932188134525	3	0 3

A:

I	COEFFICIENT	ORDER	EXPONENTS
1	-.7071067811865475	1	1 0
2	0.7071067811865475	1	0 1
3	-.7071067811865475	2	0 2
4	-.3535533905932737	3	3 0
5	-1.060660171779821	3	1 2

The deviations g_1 , g_2 , and g_3 from the conditions of symplecticity listed in eq. 47 in this case were

$$\begin{aligned}
g_1 &= -0.2220446049250313 \times 10^{-15}, \\
g_2 &= 0.2220446049250313 \times 10^{-15}, \\
g_3 &= 0.3330669073875470 \times 10^{-15}.
\end{aligned}
\tag{52}$$

Case COSY uses the first and second order aberrations out of the three orders listed here. Cases COSY_CO7 and COSY_CO7_TY0 have the same aberrations to order 3 as listed here; however, they additionally use aberrations to order 7. EXPO symplectification in *COSY INFINITY* is applied to particle coordinates during tracking and not to the aberrations.

4.1.3 Cases COSY, COSY_CO7, and COSY_CO7_TY0 (relativistic ODEs)

For reference purposes and not as part of the set of test cases, the following are aberrations of *COSY INFINITY*'s built-in electrostatic spherical deflector element ESP to order 3 calculated with relativistic equations of motion and non-relativistic energy 10^{-7} MeV.

X:

I	COEFFICIENT	ORDER	EXPONENTS
1	0.7071067812461679	1	1 0
2	0.7071067812028380	1	0 1
3	-.4999999999156844	2	2 0
4	1.000000000107354	2	1 1
5	0.2071067812063196	2	0 2
6	-.3535533905038438	3	3 0
7	0.1192400494542621E-09	3	2 1
8	0.6066017193166706E-01	3	1 2
9	0.2928932188481623	3	0 3

A:

I	COEFFICIENT	ORDER	EXPONENTS
1	-.7071067810510162	1	1 0
2	0.7071067812461679	1	0 1
3	-.7702536019579714E-15	2	2 0
4	-.5759281940243000E-15	2	1 1
5	-.7071067812028382	2	0 2
6	-.3535533904658875	3	3 0
7	0.5962026277964459E-10	3	2 1
8	-1.060660171744638	3	1 2
9	0.5962020079341501E-10	3	0 3

The deviations g_1 , g_2 , and g_3 from the conditions of symplecticity listed in eq. 47 in this case were

$$\begin{aligned}
 g_1 &= -0.1110223024625157 \times 10^{-15}, \\
 g_2 &= 0.9010236821814543 \times 10^{-16}, \\
 g_3 &= 0.2962204290179707 \times 10^{-15}.
 \end{aligned}
 \tag{53}$$

4.1.4 Case LEGACY1965

The first and second order aberrations of the electrostatic spherical deflector calculated using analytic formulas from Wollnik's paper are as follows.

X:

I	COEFFICIENT	ORDER	EXPONENTS
1	0.7071067811865476	1	1 0
2	0.7071067811865475	1	0 1
3	-.5000000000000001	2	2 0
4	0.2928932188134526	2	1 1
5	0.2071067811865476	2	0 2

A:

I	COEFFICIENT	ORDER	EXPONENTS
1	-.7071067811865475	1	1 0
2	0.7071067811865476	1	0 1
3	-.5000000000000000	2	2 0
4	-.7071067811865475	2	1 1
5	-.2071067811865475	2	0 2

The aberration formulas were transformed from Wollnik's beamline coordinates to *COSY INFINITY*'s (x, a) coordinates. The deviations g_1 , g_2 , and g_3 from the conditions of symplecticity listed in eq. 47 in this case were

$$\begin{aligned} g_1 &= 0.0000000000000000, \\ g_2 &= -0.2928932188134525, \\ g_3 &= 0.7071067811865477. \end{aligned} \tag{54}$$

4.1.5 Case GIOS

The first and second order aberrations of the electrostatic spherical deflector calculated using the program *GIOS* are as follows.

X:			
I	COEFFICIENT	ORDER EXPONENTS	
1	0.7071067812	1	1 0
2	0.7071067812	1	0 1
3	-.5000000000	2	2 0
4	0.2928932188	2	1 1
5	0.2071067812	2	0 2

A:			
I	COEFFICIENT	ORDER EXPONENTS	
1	-.7071067812	1	1 0
2	0.7071067812	1	0 1
3	-.5000000000	2	2 0
4	-.7071067812	2	1 1
5	-.2071067812	2	0 2

The aberrations were transformed from *GIOS*'s beamline coordinates to *COSY INFINITY*'s (x, a) coordinates. The deviations g_1 , g_2 , and g_3 from the conditions of symplecticity listed in eq. 47 in this case were

$$\begin{aligned} g_1 &= 3.80493 \times 10^{-11}, \\ g_2 &= -0.292893, \\ g_3 &= 0.707107. \end{aligned} \tag{55}$$

4.1.6 Case LEGACY1965_Mod

The first and second order aberrations of the electrostatic spherical deflector calculated using analytic formulas from Wollnik's paper with our modifications to account for a hard edge fringe field made by Valetov (in this volume) are as follows.

X:			
I	COEFFICIENT	ORDER EXPONENTS	
1	0.7071067811865476	1	1 0
2	0.7071067811865475	1	0 1
3	-.50000000000000001	2	2 0
4	1.0000000000000000	2	1 1
5	0.2071067811865476	2	0 2

A:			
I	COEFFICIENT	ORDER EXPONENTS	
1	-.7071067811865475	1	1 0

2	0.7071067811865476	1	0	1
3	-.7071067811865475	2	0	2

The aberration formulas were transformed from Wollnik's beamline coordinates to *COSY INFINITY*'s (x, a) coordinates. The deviations g_1 , g_2 , and g_3 from the conditions of symplecticity listed in eq. 47 in this case were

$$\begin{aligned}
 g_1 &= 0.0000000000000000, \\
 g_2 &= -2.220446049250313 \times 10^{-16}, \\
 g_3 &= 1.110223024625157 \times 10^{-16}.
 \end{aligned}
 \tag{56}$$

4.2 Electrostatic Cylindrical Deflector Aberrations

4.2.1 Case EDABRT

The first and second order aberrations of the electrostatic cylindrical deflector calculated using the analytic formulas of eqns. 44-45 are as follows.

X:				
I	COEFFICIENT	ORDER	EXPONENTS	
1	0.4440158403262133	1	1	0
2	0.6335810656653995	1	0	1
3	-1.029322282408272	2	2	0
4	0.4452197131126670	2	1	1
5	0.9767302144879608E-01	2	0	2
A:				
I	COEFFICIENT	ORDER	EXPONENTS	
1	-1.267162131330799	1	1	0
2	0.4440158403262133	1	0	1
3	-.3987403747459332	2	2	0
4	-.3499052358016756	2	1	1
5	-.7510014111251326	2	0	2

The deviations g_1 , g_2 , and g_3 from the conditions of symplecticity listed in eq. 47 in this case were

$$\begin{aligned}
 g_1 &= 0.0000000000000000, \\
 g_2 &= 0.0000000000000000, \\
 g_3 &= 1.387778780781446 \times 10^{-16}.
 \end{aligned}
 \tag{57}$$

4.2.2 Cases COSY, COSY_CO7, and COSY_CO7_TY0

The aberrations of *COSY INFINITY*'s built-in electrostatic cylindrical deflector element ECL to order 3 calculated with non-relativistic equations of motion are as follows.

X:				
I	COEFFICIENT	ORDER	EXPONENTS	
1	0.4440158403262133	1	1	0
2	0.6335810656653997	1	0	1
3	-1.029322282408272	2	2	0
4	0.4452197131126671	2	1	1
5	0.9767302144879608E-01	2	0	2
6	-.9310536195454117	3	3	0

7	-.7814348139394898	3	2	1
8	-.7214969045085790	3	1	2
9	0.1172683765076182	3	0	3

A:

I	COEFFICIENT	ORDER	EXPONENTS	
1	-1.267162131330799	1	1	0
2	0.4440158403262133	1	0	1
3	-.3987403747459333	2	2	0
4	-.3499052358016756	2	1	1
5	-.7510014111251326	2	0	2
6	-.6758776475462280	3	3	0
7	-.2919765941781459	3	2	1
8	-1.233526213798173	3	1	2
9	-.2301781799921575	3	0	3

The deviations g_1 , g_2 , and g_3 from the conditions of symplecticity listed in eq. 47 in this case were

$$\begin{aligned}
 g_1 &= 0.4440892098500626 \times 10^{-15}, \\
 g_2 &= 0.2220446049250313 \times 10^{-15}, \\
 g_3 &= 0.2498001805406602 \times 10^{-15}.
 \end{aligned}
 \tag{58}$$

Case COSY uses the first and second order aberrations out of the three orders listed here. Cases COSY_CO7 and COSY_CO7_TY0 have the same aberrations to order 3 as listed here; however, they additionally use aberrations to order 7. EXPO symplectification in *COSY INFINITY* is applied to particle coordinates during tracking and not to the aberrations.

4.2.3 Cases COSY, COSY_CO7, and COSY_CO7_TY0 (relativistic ODEs)

For reference purposes and not as part of the set of test cases, the following are aberrations of *COSY INFINITY*'s built-in electrostatic cylindrical deflector element ECL to order 3 calculated with relativistic equations of motion and non-relativistic energy 10^{-7} MeV.

X:

I	COEFFICIENT	ORDER	EXPONENTS	
1	0.4440158403796342	1	1	0
2	0.6335810656806897	1	0	1
3	-1.029322282295397	2	2	0
4	0.4452197132275977	2	1	1
5	0.9767302147275347E-01	2	0	2
6	-.9310536194141522	3	3	0
7	-.7814348137898871	3	2	1
8	-.7214969043552069	3	1	2
9	0.1172683765442521	3	0	3

A:

I	COEFFICIENT	ORDER	EXPONENTS	
1	-1.267162131225344	1	1	0
2	0.4440158403796342	1	0	1
3	-.3987403746497010	2	2	0
4	-.3499052357127290	2	1	1
5	-.7510014111067631	2	0	2

6	-.6758776475027084	3	3	0
7	-.2919765941199486	3	2	1
8	-1.233526213775116	3	1	2
9	-.2301781799487691	3	0	3

The deviations g_1 , g_2 , and g_3 from the conditions of symplecticity listed in eq. 47 in this case were

$$\begin{aligned}
 g_1 &= 0.4440892098500626 \times 10^{-15}, \\
 g_2 &= 0.4440892098500626 \times 10^{-15}, \\
 g_3 &= 0.4163336342344337 \times 10^{-15}.
 \end{aligned}
 \tag{59}$$

4.2.4 Case LEGACY1965

The first and second order aberrations of the electrostatic cylindrical deflector calculated using analytic formulas from Wollnik's paper are as follows.

X:				
I	COEFFICIENT	ORDER	EXPONENTS	
1	0.4440158403262133	1	1	0
2	0.6335810656653995	1	0	1
3	-1.029322282408272	2	2	0
4	-.1883613525527325	2	1	1
5	0.9767302144879608E-01	2	0	2
A:				
I	COEFFICIENT	ORDER	EXPONENTS	
1	-1.267162131330799	1	1	0
2	0.4440158403262133	1	0	1
3	-.9613804333183333	2	2	0
4	-1.399620943206702	2	1	1
5	-.4696813818389327	2	0	2

The aberration formulas were transformed from Wollnik's beamline coordinates to *COSY INFINITY*'s (x, a) coordinates. The deviations g_1 , g_2 , and g_3 from the conditions of symplecticity listed in eq. 47 in this case were

$$\begin{aligned}
 g_1 &= 0.0000000000000000, \\
 g_2 &= -0.5559841596737869, \\
 g_3 &= 0.6335810656653996.
 \end{aligned}
 \tag{60}$$

4.2.5 Case GIOS

The first and second order aberrations of the electrostatic cylindrical deflector calculated using the program *GIOS* are as follows.

X:				
I	COEFFICIENT	ORDER	EXPONENTS	
1	0.4440158574	1	1	0
2	0.6335810705	1	0	1
3	-1.029322250	2	2	0
4	-.1883613764	2	1	1
5	0.9767302679E-01	2	0	2

A:

I	COEFFICIENT	ORDER	EXPONENTS
1	-1.267162098	1	1 0
2	0.4440158574	1	0 1
3	-.9613804652	2	2 0
4	-1.399620967	2	1 1
5	-.4696813690	2	0 2

The aberrations were transformed from *GIOS*'s beamline coordinates to *COSY INFINITY*'s (x, a) coordinates. The deviations g_1 , g_2 , and g_3 from the conditions of symplecticity listed in eq. 47 in this case were

$$\begin{aligned} g_1 &= 1.70523 \times 10^{-10}, \\ g_2 &= -0.555984 \\ g_3 &= 0.633581. \end{aligned} \tag{61}$$

4.2.6 Case LEGACY1965_Mod

The first and second order aberrations of the electrostatic cylindrical deflector calculated using analytic formulas from Wollnik's paper with our modifications to account for a hard edge fringe field made by Valetov (in this volume) are as follows.

X:

I	COEFFICIENT	ORDER	EXPONENTS
1	0.4440158403262133	1	1 0
2	0.6335810656653995	1	0 1
3	-1.029322282408272	2	2 0
4	0.4452197131126670	2	1 1
5	0.9767302144879608E-01	2	0 2

A:

I	COEFFICIENT	ORDER	EXPONENTS
1	-1.267162131330799	1	1 0
2	0.4440158403262133	1	0 1
3	-.3987403747459332	2	2 0
4	-.3499052358016756	2	1 1
5	-.7510014111251326	2	0 2

The aberration formulas were transformed from Wollnik's beamline coordinates to *COSY INFINITY*'s (x, a) coordinates. The deviations g_1 , g_2 , and g_3 from the conditions of symplecticity listed in eq. 47 in this case were

$$\begin{aligned} g_1 &= 0.0000000000000000, \\ g_2 &= 0.0000000000000000, \\ g_3 &= 1.387778780781446 \times 10^{-16}. \end{aligned} \tag{62}$$

4.3 Comparison of Particle Tracking Results

Tracking for a drift-deflector-drift cell For each aberration calculation method considered in this section, using the particle tracking methods of *COSY INFINITY* applied to transfer maps calculated by *ESCP010AIEP.FOX*, we tracked a particle bunch for 10000 turns through a cell consisting of a drift, a 45° electrostatic spherical or cylindrical deflector of radius 1 m, and another drift of the same length as the first drift. Doing so is useful for a visual comparison of the cases as errors in the second order matrix

elements quickly reveal themselves as non-physical effects, as well as for numerical comparison of the particle coordinate errors. Figs. 1–4 and 5–8 show the results for the electrostatic and cylindrical deflector cases, respectively. For comparable rates of amplitude growth with aberrations to second order (or equivalently, with computation order 2), each drift was 1.5 m in all electrostatic spherical deflector cases and 0.5 m in all electrostatic cylindrical deflector cases.

The normal form amplitude A_{NF} plotted in these figures is the vector length $\|(x_{\text{NF}}, a_{\text{NF}})\|_2$ of the normal form coordinates $(x_{\text{NF}}, a_{\text{NF}})$, which are obtained using the relation

$$\begin{pmatrix} x_{\text{NF}} \\ a_{\text{NF}} \end{pmatrix} = \frac{1}{\sqrt{\beta}} \begin{pmatrix} 1 & 0 \\ \alpha & \beta \end{pmatrix} \begin{pmatrix} x \\ a \end{pmatrix}, \quad (63)$$

where α and β are the Twiss parameters computed from the linear transfer map. (By “normal form” we mean the linear normal form in this work; see Berz (1999) for the nonlinear normal form theory.)

Tracking plots for Case LEGACY1965 are visually identical to those of Case GIOS, which is because *GIOS* uses aberration formulas from Wollnik’s paper. As the analysis by Valetov (in this volume) shows, the aberration formulas in Wollnik’s paper are correct only for the main field, and we checked that after scaling of initial and final coordinates in Wollnik’s notation to account for a hard edge fringe field they agree with aberration formulas in eqns. 44–45 and with *COSY INFINITY*. Accordingly, plots for Case LEGACY1965_Mod are visually identical to those of Cases COSY and EDABRT. Demonstrating the inaccuracy of Cases LEGACY1965 and GIOS, the normal form amplitudes for these aberrations diverge to infinity significantly faster than for the other methods.

As Figs. 9 and 10 show, in Cases EDABRT, COSY, and LEGACY1965_Mod, errors in normal form amplitude grow cubically with increasing normal form amplitude in the x – a plane, corresponding to the aberrations being valid to second order. On the other hand, because the second order aberrations from Wollnik’s paper and *GIOS* are only valid for the main field and not the deflector as a whole without additionally accounting for a fringe field, and only first order aberrations are valid without doing so, in Cases LEGACY1965 and GIOS errors in normal form amplitude grow quadratically with increasing normal form amplitude. Considering that the truncation errors of computation order 7 are insignificant compared to computation order 2, Case COSY_CO7 was used as the reference case in the calculation of the errors in this comparison. (We remark that Valetov et al. (in print) compared electrostatic spherical deflector transfer maps computed numerically using *COSY INFINITY* and analytically using Kepler theory, and found an agreement between the respective transfer map elements to nearly machine precision.)

The normal form amplitudes in Cases COSY_CO7 and COSY_CO7_TY0 are stable around the initial amplitudes and visually form horizontal lines, with some exceptions of the outermost particles. This effect is particularly expressed with symplectification, as demonstrated by Case COSY_CO7_TY0. This demonstrates the advantages of high order transfer map tracking and symplectification.

Tracking for a deflector without drifts We also tracked particles for 10000 turns through a cell defined as a 45° electrostatic spherical or cylindrical deflector of radius 1 m, with aberrations computed using each of the compared methods. Figs. 11–14 and 15–18 show the results of this tracking for the spherical and the cylindrical deflector, respectively. For this cell, in Cases LEGACY1965 and GIOS, scaling to account for the hard edge fringe field was performed at the entrance edge of the deflector in the first turn and at the exit edge of the deflector in the last turn for each plotted data point, based on the idea that the composition of consecutive scaling and descaling for the hard edge fringe field is identity to any computation order. However, such partial, separate (“PS”) scaling is not equivalent to using electrostatic deflector aberrations that account for both the main field and the fringe field.

The transfer map of a 360° electrostatic spherical deflector is identity, and for each computation order, the composition of eight identical 45° electrostatic spherical deflectors is also identity in the differential algebra of that order. One may expect for a 45° electrostatic spherical deflector that the normal form amplitude will have a period of eight turns in calculations of any order, including the second order. However, this is not the case because tracking particles using one transfer map of a finite order j for n turns is not the same as tracking particles using an n -times composition of this transfer map. This is because the former is essentially

a composition of n polynomial functions of order j , which results in a polynomial function of order nj that is applied to particle coordinates. On the other hand, the latter is essentially an application of one polynomial function of order n to particle coordinates.

Similarly, although one may expect that with PS scaling the tracking pictures for Cases LEGACY1965 and GIOS would become identical to those of Cases EDABRT, COSY, and LEGACY1965_Mod, this is not the case. Respectively, Figs. 19 and 20 show that PS scaling results in lower orders of error growths in the normal form amplitude with increasing normal form amplitude compared to Case LEGACY1965_Mod, indicating that the former has a lower accuracy than the latter.

In general, there is a distinction between tracking particles using a composition of DA transfer maps and the same DA transfer maps individually, which is particularly important at low computation orders, whereas at higher computation orders (e.g. order 7) the difference tends to become negligible. These considerations are not specific to DA transfer maps and also apply to aberrations of a finite order for a series of particle optical elements compared to using aberrations of the same order for each of these elements, as well as to truncated power series algebra (TPSA) transfer maps.

For particle tracking in Case COSY_CO7, because its computation order is 7, the errors in the coordinates are expected to have the order of growth 8 in function of the initial coordinates. This order of growth consideration is particularly trivial to demonstrate on the example of the electrostatic spherical deflector. The exact transfer map of a 360° electrostatic spherical deflector is identity, which is why without any truncation errors the tracking picture in Fig. 21 would show periodic motion for each particle with period 8. Consider the visually continuous piecewise linear arc traced in every 8th turn by the particle with the initial normal form x coordinate $x_{\text{NF}} = 0.22 \text{ m}^{1/2}$. The length of this error arc is $8.68 \times 10^{-3} \text{ m}^{1/2}$, so for the next particle with initial coordinate $x_{\text{NF}} = 0.24 \text{ m}^{1/2}$ we would expect the error arc length to be about $8.68 \times 10^{-3} (0.24/0.22)^8 \text{ m}^{1/2} = 1.74 \times 10^{-2} \text{ m}^{1/2}$, which quite accurately approximates its measured length $1.72 \times 10^{-2} \text{ m}^{1/2}$.

Similarly to what was observed for the cell with drifts, the normal form amplitude in Cases COSY_CO7 and COSY_CO7_TY0 is stable around the initial amplitude, with some exceptions of the outermost particles, and this effect is particularly expressed with symplectification, as demonstrated by Case COSY_CO7_TY0.

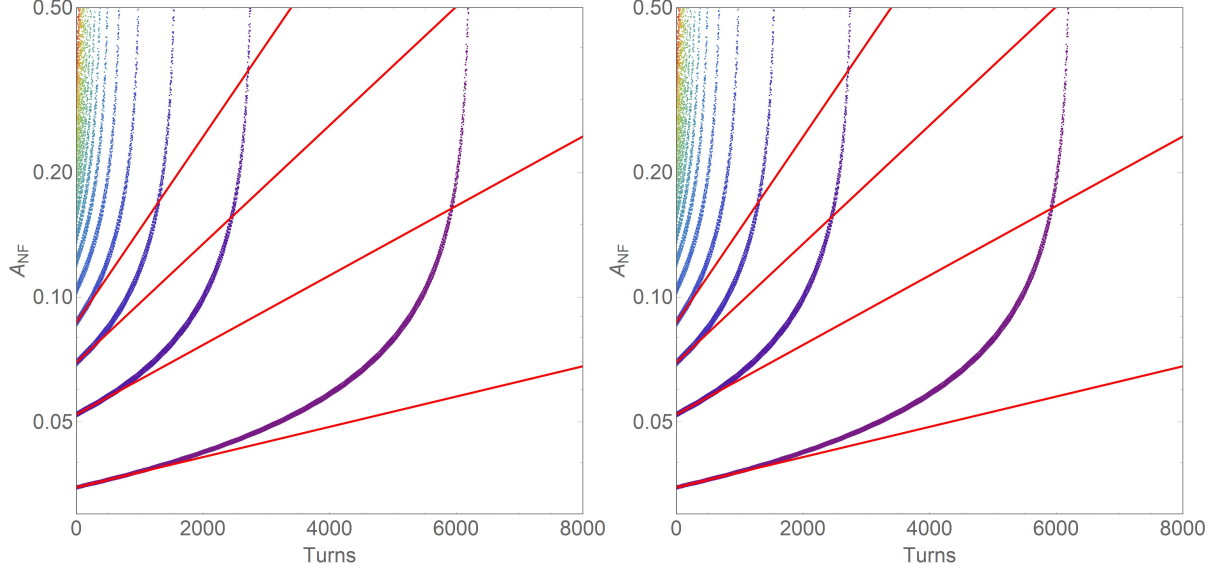


Figure 1: Cases EDABRT (left) and COSY (right) for the cell of the 45° degree electrostatic spherical deflector of radius 1 m between two 1.5 m drifts. The normal form horizontal transverse amplitude $A_{\text{NF}} [\text{m}^{1/2}]$ versus the number of turns. The initial normal form coordinates of the particles were $(x_{\text{NF}}, a_{\text{NF}}) = (1.74 \times 10^{-2} \text{ m}^{1/2}, 0) \cdot j$ for $j = 2, 3, \dots, 20$. The logarithmic slopes of A_{NF} for the innermost four particles are 8.41×10^{-5} , 1.93×10^{-4} , 3.30×10^{-4} , and 5.16×10^{-4} (both left and right).

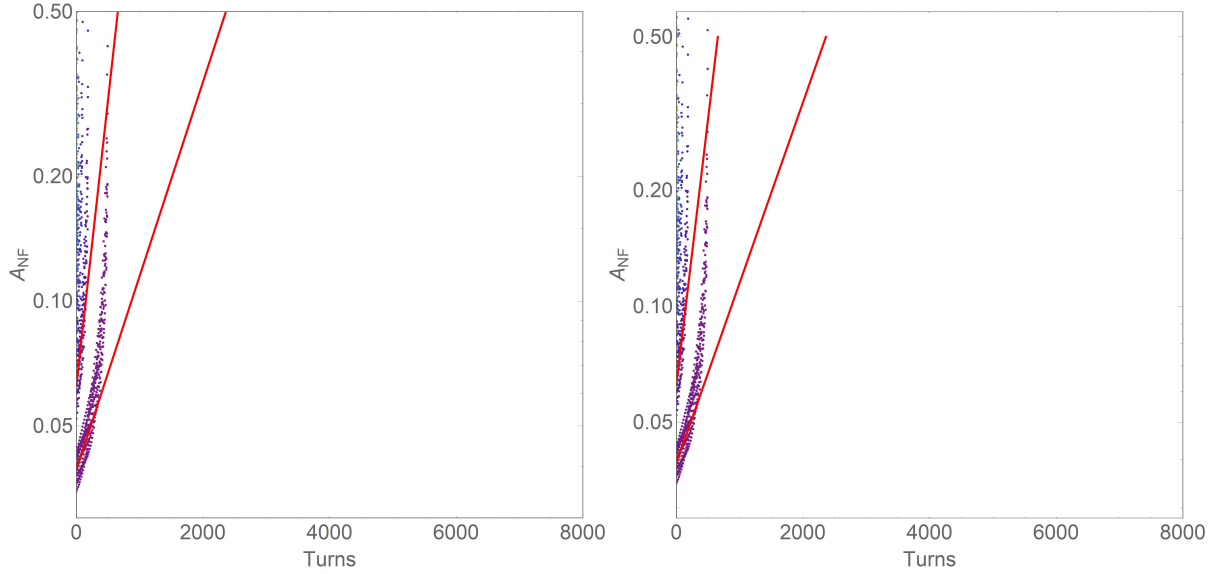


Figure 2: Cases LEGACY1965 (left) and GIOS (right) for the cell of the 45° degree electrostatic spherical deflector of radius 1 m between two 1.5 m drifts. The normal form horizontal transverse amplitude $A_{\text{NF}} [\text{m}^{1/2}]$ versus the number of turns. The initial normal form coordinates of the particles were $(x_{\text{NF}}, a_{\text{NF}}) = (1.74 \times 10^{-2} \text{ m}^{1/2}, 0) \cdot j$ for $j = 2, 3, \dots, 20$. The logarithmic slopes of A_{NF} for the innermost two particles are 1.08×10^{-3} and 3.18×10^{-3} (both left and right).

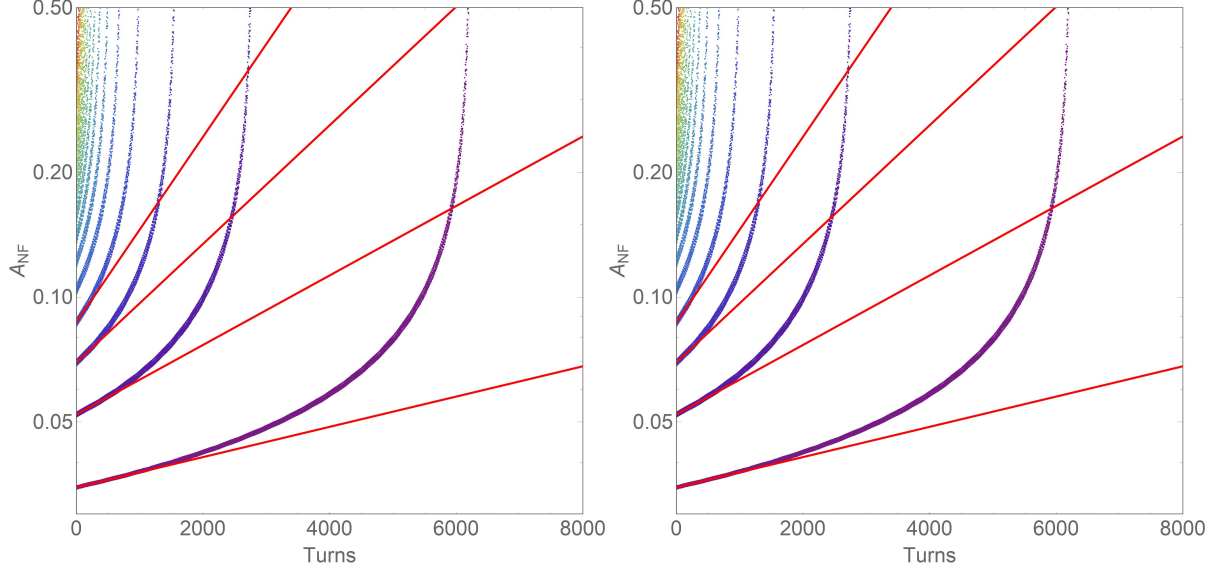


Figure 3: Cases LEGACY1965_Mod (left) and EDABRT (right) for the cell of the 45° degree electrostatic spherical deflector of radius 1 m between two 1.5 m drifts. The normal form horizontal transverse amplitude A_{NF} [$\text{m}^{1/2}$] versus the number of turns. The initial normal form coordinates of the particles were $(x_{\text{NF}}, a_{\text{NF}}) = (1.74 \times 10^{-2} \text{ m}^{1/2}, 0) \cdot j$ for $j = 2, 3, \dots, 20$. The logarithmic slopes of A_{NF} for the innermost four particles are 8.41×10^{-5} , 1.93×10^{-4} , 3.30×10^{-4} , and 5.16×10^{-4} (both left and right).

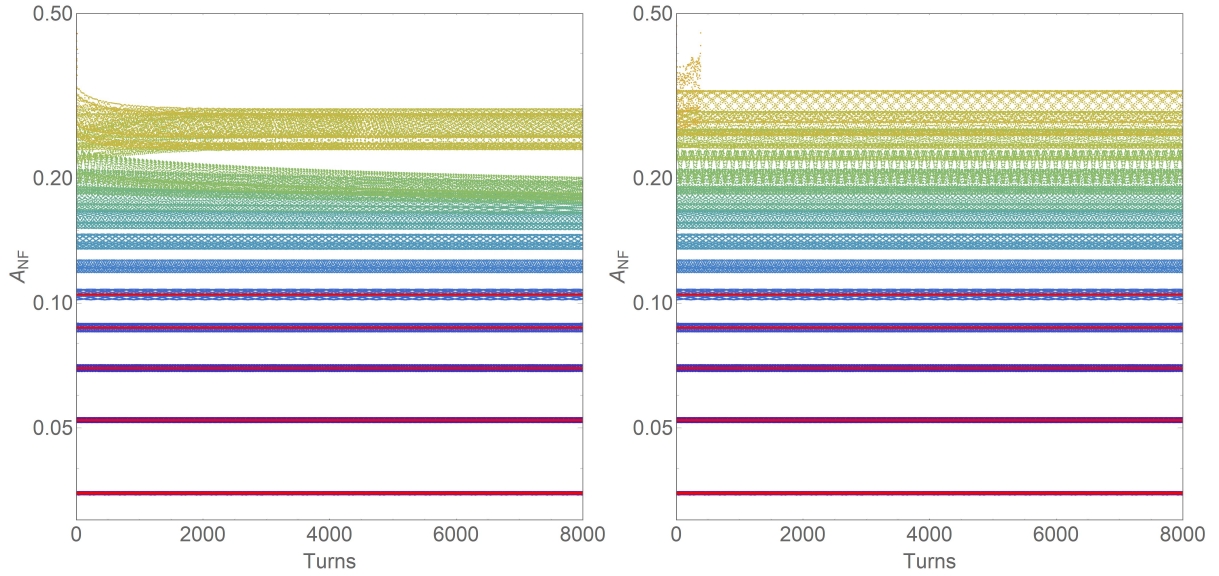


Figure 4: Cases COSY_CO7 (left) and COSY_CO7_TY0 (right) for the cell of the 45° degree electrostatic spherical deflector of radius 1 m between two 1.5 m drifts. The normal form horizontal transverse amplitude A_{NF} [$\text{m}^{1/2}$] versus the number of turns. The initial normal form coordinates of the particles were $(x_{\text{NF}}, a_{\text{NF}}) = (1.74 \times 10^{-2} \text{ m}^{1/2}, 0) \cdot j$ for $j = 2, 3, \dots, 20$. The logarithmic slopes of A_{NF} for the innermost five particles are -6.76×10^{-11} , 1.10×10^{-8} , 7.11×10^{-9} , 2.05×10^{-8} , 1.27×10^{-8} (left) and -6.61×10^{-11} , 1.10×10^{-8} , 7.57×10^{-9} , 2.37×10^{-8} , 2.93×10^{-8} (right).

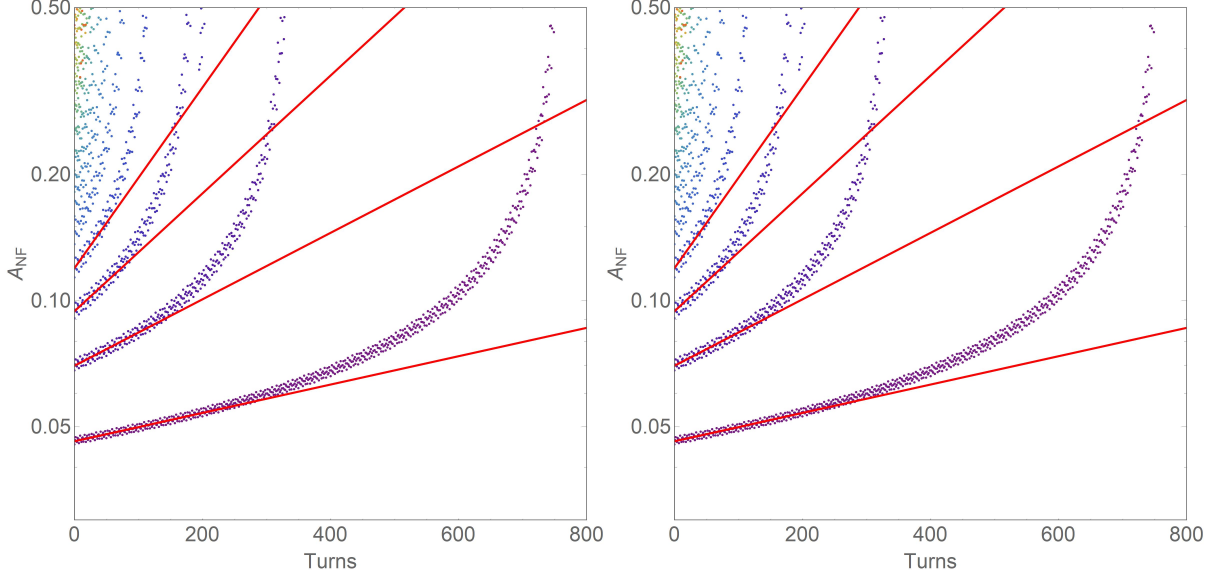


Figure 5: Cases EDABRT (left) and COSY (right) for the cell of the 45° degree electrostatic cylindrical deflector of radius 1m between two 0.5m drifts. The normal form horizontal transverse amplitude A_{NF} [$\text{m}^{1/2}$] versus the number of turns. The initial normal form coordinates of the particles were $(x_{\text{NF}}, a_{\text{NF}}) = (2.27 \times 10^{-2} \text{ m}^{1/2}, 0) \cdot j$ for $j = 2, 3, \dots, 20$. The logarithmic slopes of A_{NF} for the innermost four particles are 7.79×10^{-4} , 1.83×10^{-3} , 3.24×10^{-3} , and 4.96×10^{-3} (both left and right).

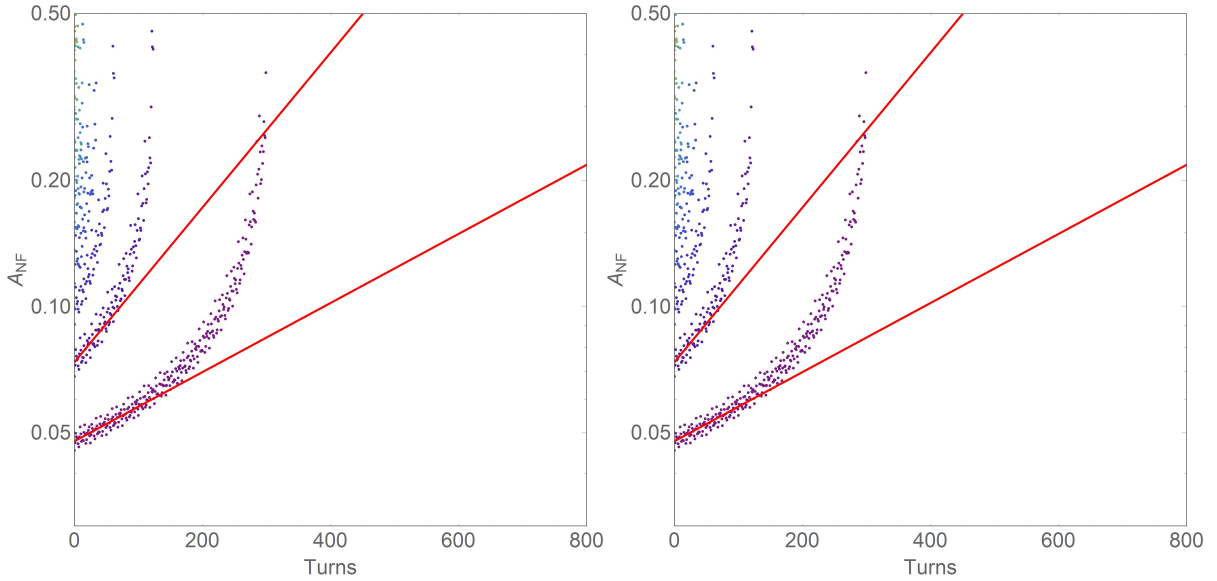


Figure 6: Cases LEGACY1965 (left) and GIOS (right) for the cell of the 45° degree electrostatic cylindrical deflector of radius 1m between two 0.5m drifts. The normal form horizontal transverse amplitude A_{NF} [$\text{m}^{1/2}$] versus the number of turns. The initial normal form coordinates of the particles were $(x_{\text{NF}}, a_{\text{NF}}) = (2.27 \times 10^{-2} \text{ m}^{1/2}, 0) \cdot j$ for $j = 2, 3, \dots, 20$. The logarithmic slopes of A_{NF} for the innermost two particles are 1.90×10^{-3} and 4.25×10^{-3} (both left and right).

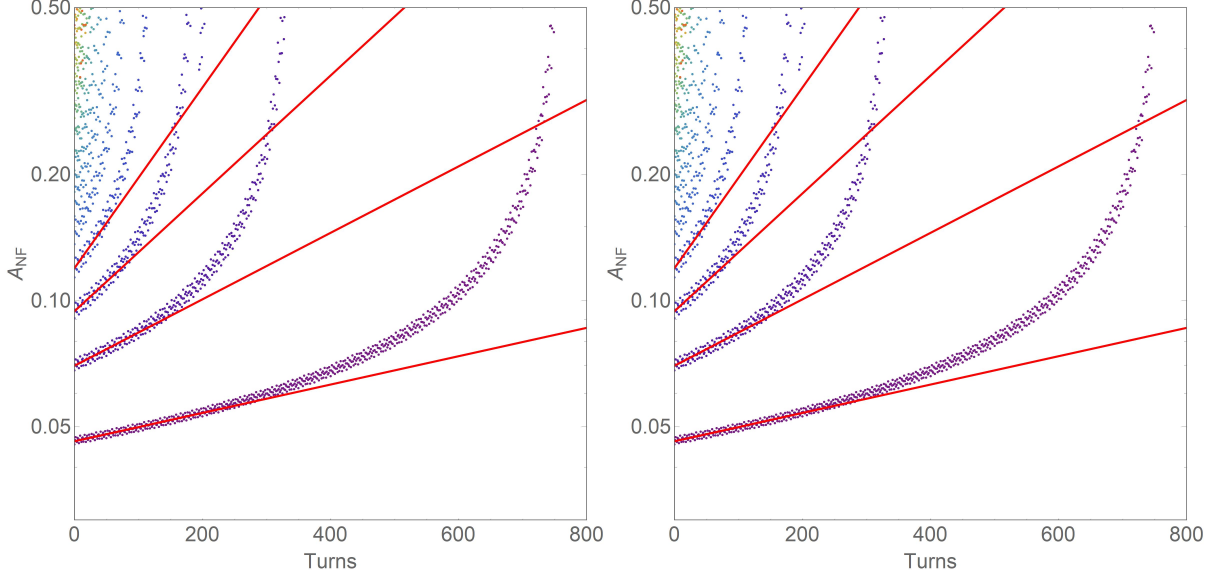


Figure 7: Cases LEGACY1965_Mod (left) and EDABRT (right) for the cell of the 45° degree electrostatic cylindrical deflector of radius 1 m between two 0.5 m drifts. The normal form horizontal transverse amplitude A_{NF} [$\text{m}^{1/2}$] versus the number of turns. The initial normal form coordinates of the particles were $(x_{\text{NF}}, a_{\text{NF}}) = (2.27 \times 10^{-2} \text{ m}^{1/2}, 0) \cdot j$ for $j = 2, 3, \dots, 20$. The logarithmic slopes of A_{NF} for the innermost four particles are 7.79×10^{-4} , 1.83×10^{-3} , 3.24×10^{-3} , and 4.96×10^{-3} (both left and right).

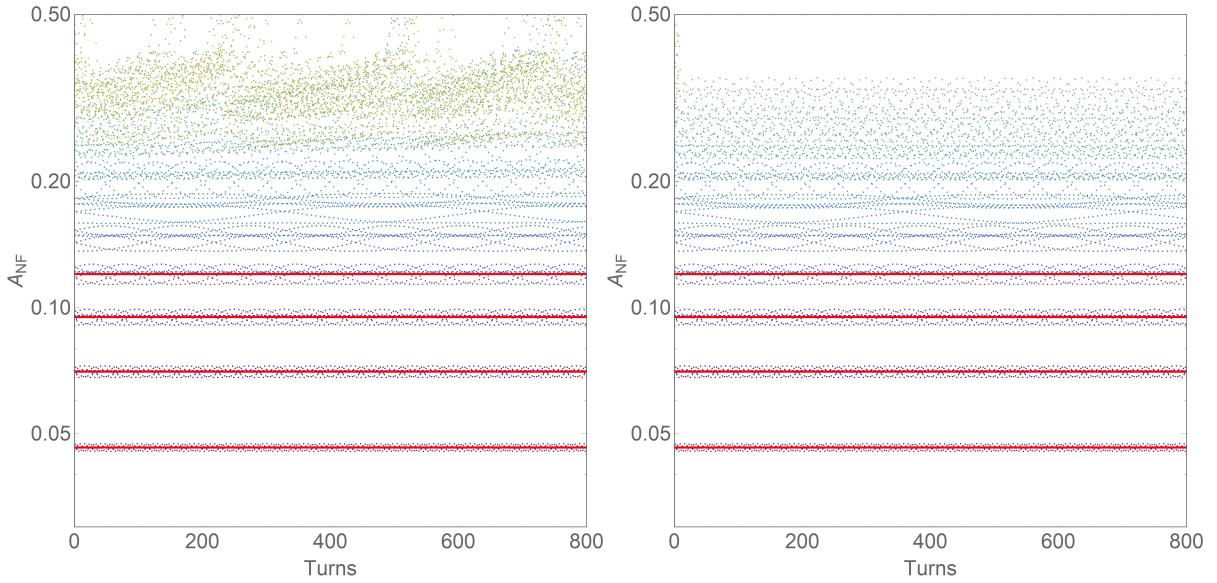


Figure 8: Cases COSY_CO7 (left) and COSY_CO7_TY0 (right) for the cell of a 45° degree electrostatic cylindrical deflector of radius 1 m between two 0.5 m drifts. The normal form horizontal transverse amplitude A_{NF} [$\text{m}^{1/2}$] versus the number of turns. The initial normal form coordinates of the particles were $(x_{\text{NF}}, a_{\text{NF}}) = (2.27 \times 10^{-2} \text{ m}^{1/2}, 0) \cdot j$ for $j = 2, 3, \dots, 20$. The logarithmic slopes of A_{NF} for the innermost four particles are 2.93×10^{-10} , 4.63×10^{-9} , 3.40×10^{-8} , 2.02×10^{-7} (left) and 2.03×10^{-10} , 2.03×10^{-9} , 3.94×10^{-9} , -7.06×10^{-9} (right).

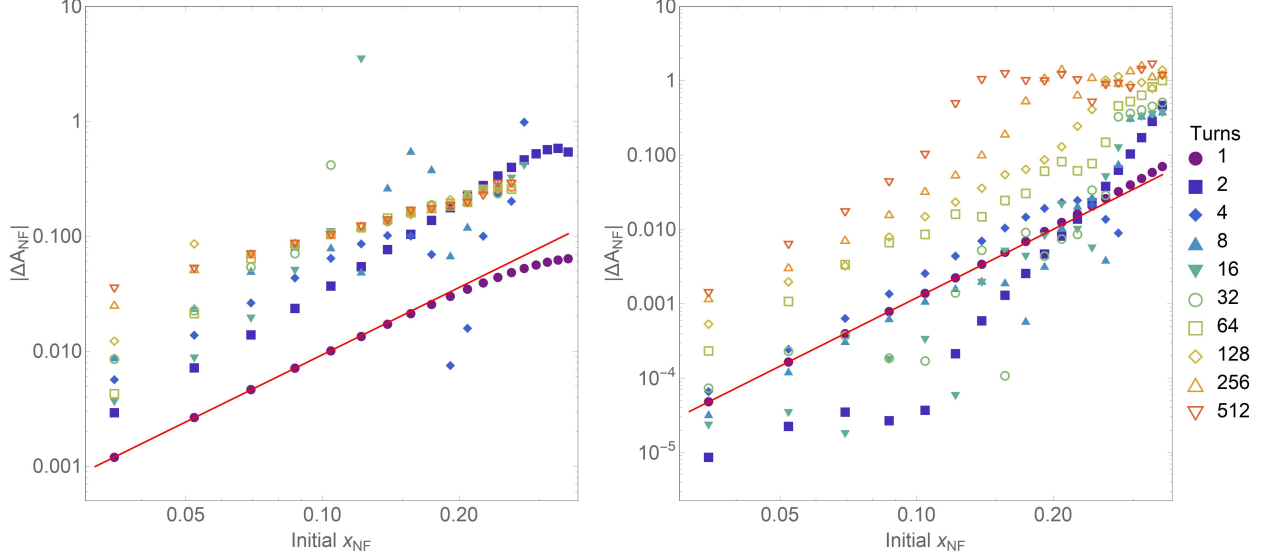


Figure 9: Cases LEGACY1965 (left) and LEGACY1965_Mod (right) for the cell of a 45° degree electrostatic spherical deflector of radius 1 m between two 1.5 m drifts. Absolute values $|\Delta A_{NF}|$ of errors in the normal form horizontal transverse amplitude A_{NF} versus the initial normal form coordinates $(x_{NF}, 0)$ are shown for 2^j tracked turns, where $j = 0, 1, \dots, 9$. The error slopes are plotted for the first turn and are 1.94 for Case LEGACY1965 and 3.06 for Case LEGACY1965_Mod. The units of normal form coordinates are $m^{1/2}$. The initial normal form coordinates of the particles were $(x_{NF}, a_{NF}) = (1.74 \times 10^{-2} m^{1/2}, 0) \cdot j$ for $j = 2, 3, \dots, 20$.

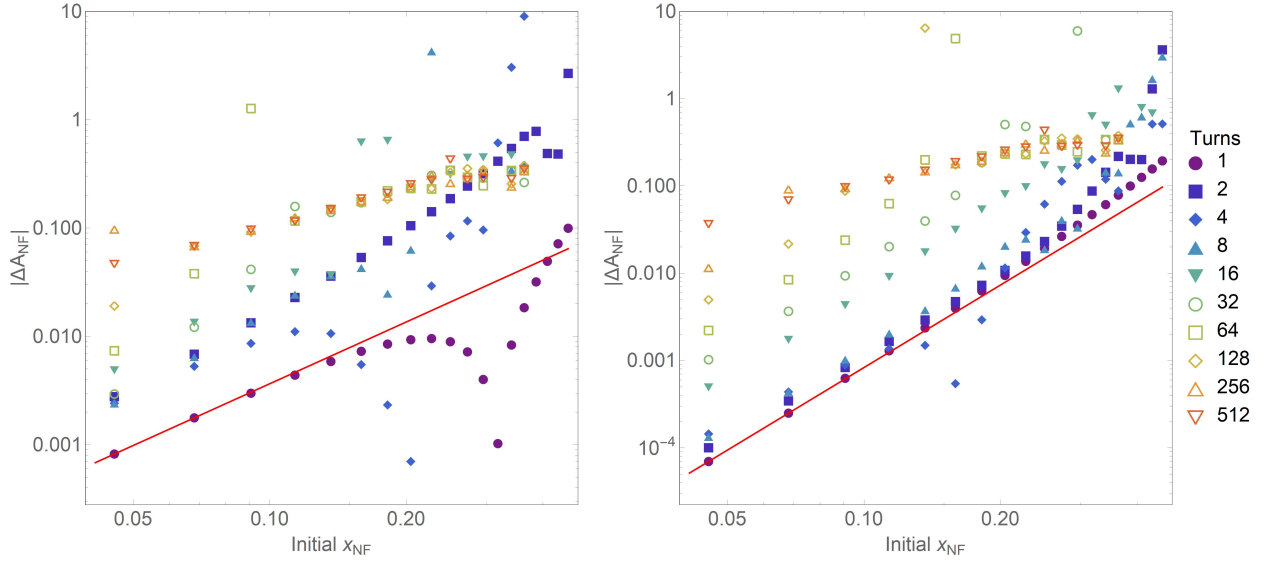


Figure 10: Cases LEGACY1965 (left) and LEGACY1965_Mod (right) for the cell of a 45° degree electrostatic cylindrical deflector of radius 1 m between two 0.5 m drifts. Absolute values $|\Delta A_{NF}|$ of errors in the normal form horizontal transverse amplitude A_{NF} versus the initial normal form coordinates $(x_{NF}, 0)$ are shown for 2^j tracked turns, where $j = 0, 1, \dots, 9$. The error slopes are plotted for the first turn and are 1.89 for Case LEGACY1965 and 3.14 for Case LEGACY1965_Mod. The units of normal form coordinates are $m^{1/2}$. The initial normal form coordinates of the particles were $(x_{NF}, a_{NF}) = (2.27 \times 10^{-2} m^{1/2}, 0) \cdot j$ for $j = 2, 3, \dots, 20$.

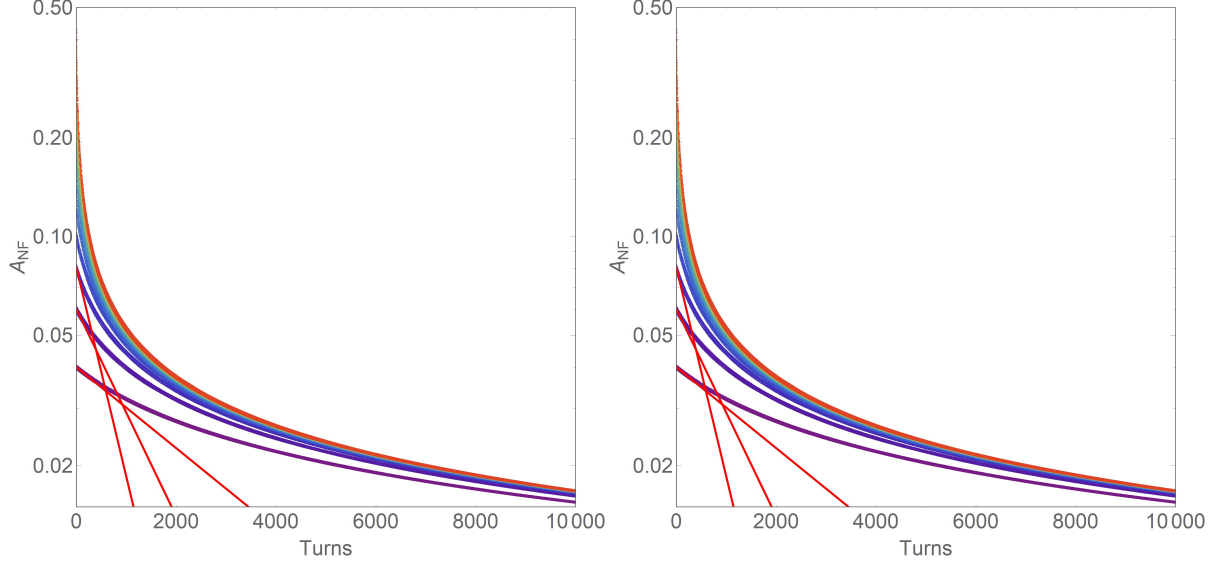


Figure 11: Cases EDABRT (left) and COSY (right) for the cell defined as the 45° degree electrostatic spherical deflector of radius 1 m. The normal form horizontal transverse amplitude A_{NF} [$\text{m}^{1/2}$] versus the number of turns. The initial normal form coordinates of the particles were $(x_{\text{NF}}, a_{\text{NF}}) = (0.02 \text{ m}^{1/2}, 0) \cdot j$ for $j = 2, 3, \dots, 20$. The logarithmic slopes of A_{NF} for the innermost three particles are -2.85×10^{-4} , -7.29×10^{-4} , and -1.47×10^{-3} (both left and right).

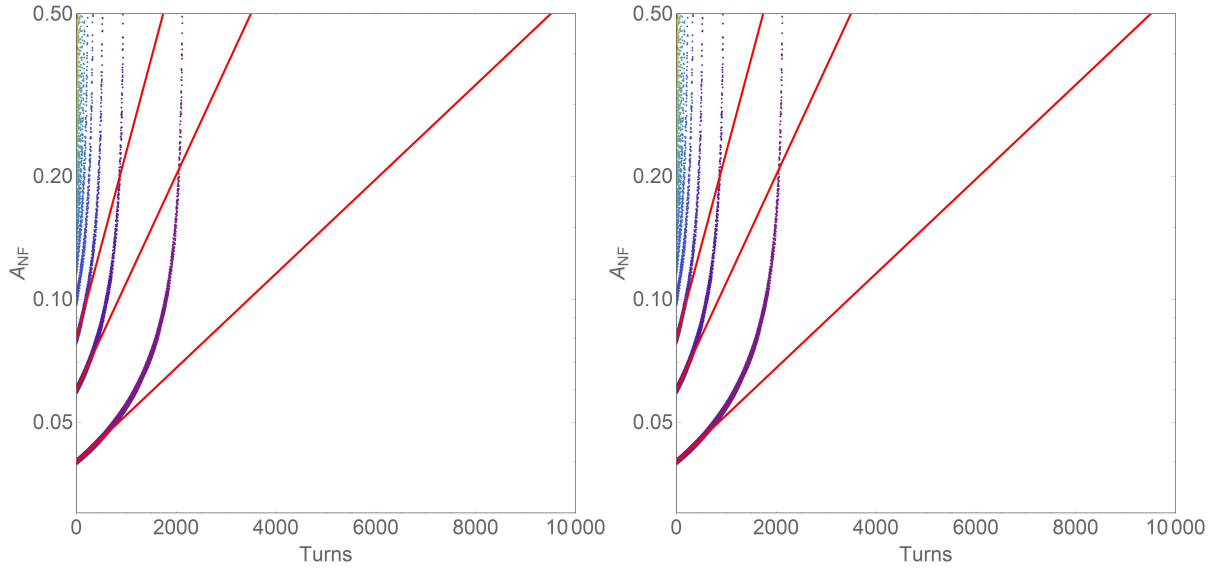


Figure 12: Cases LEGACY1965 (left) and GIOS (right) for the cell defined as the 45° degree electrostatic spherical deflector of radius 1 m. For every plotted point, scaling and descaling for a hard edge fringe field was performed for the initial coordinates in the first turn and the final coordinates in the last turn, respectively. The normal form horizontal transverse amplitude A_{NF} [$\text{m}^{1/2}$] versus the number of turns. The initial normal form coordinates of the particles were $(x_{\text{NF}}, a_{\text{NF}}) = (0.02 \text{ m}^{1/2}, 0) \cdot j$ for $j = 2, 3, \dots, 20$. The logarithmic slopes of A_{NF} for the innermost three particles are 2.66×10^{-4} , 6.07×10^{-4} , and 1.05×10^{-3} (both left and right).

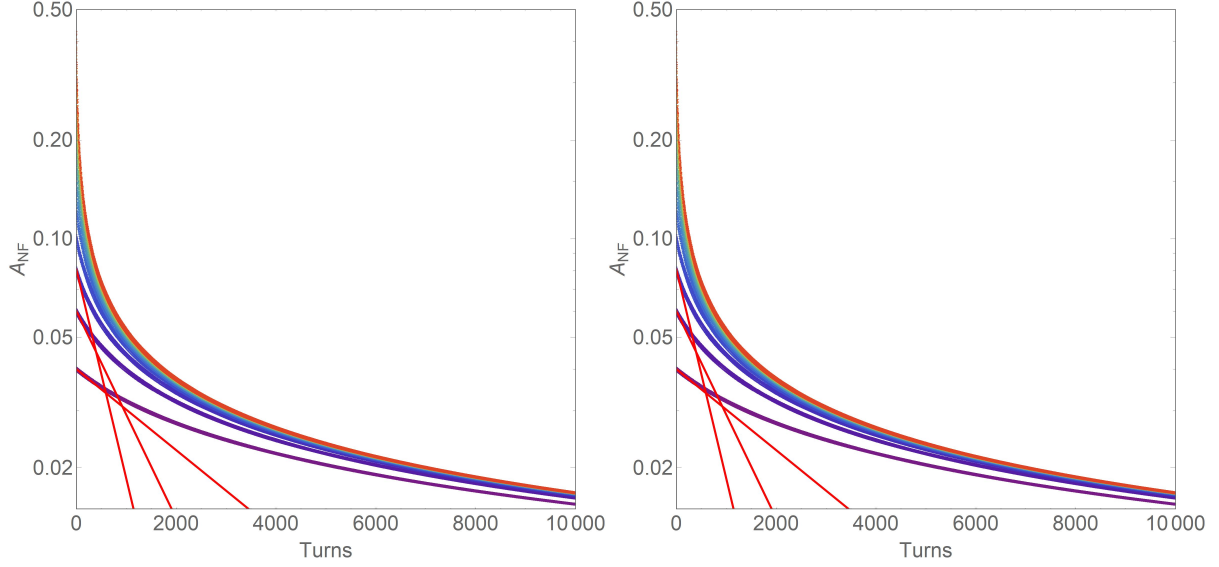


Figure 13: Cases LEGACY1965_Mod (left) and EDABRT (right) for the cell defined as the 45° degree electrostatic spherical deflector of radius 1 m. The normal form horizontal transverse amplitude A_{NF} [$\text{m}^{1/2}$] versus the number of turns. The initial normal form coordinates of the particles were $(x_{\text{NF}}, a_{\text{NF}}) = (0.02 \text{ m}^{1/2}, 0) \cdot j$ for $j = 2, 3, \dots, 20$. The logarithmic slopes of A_{NF} for the innermost three particles are -2.85×10^{-4} , -7.29×10^{-4} , and -1.47×10^{-3} (both left and right).

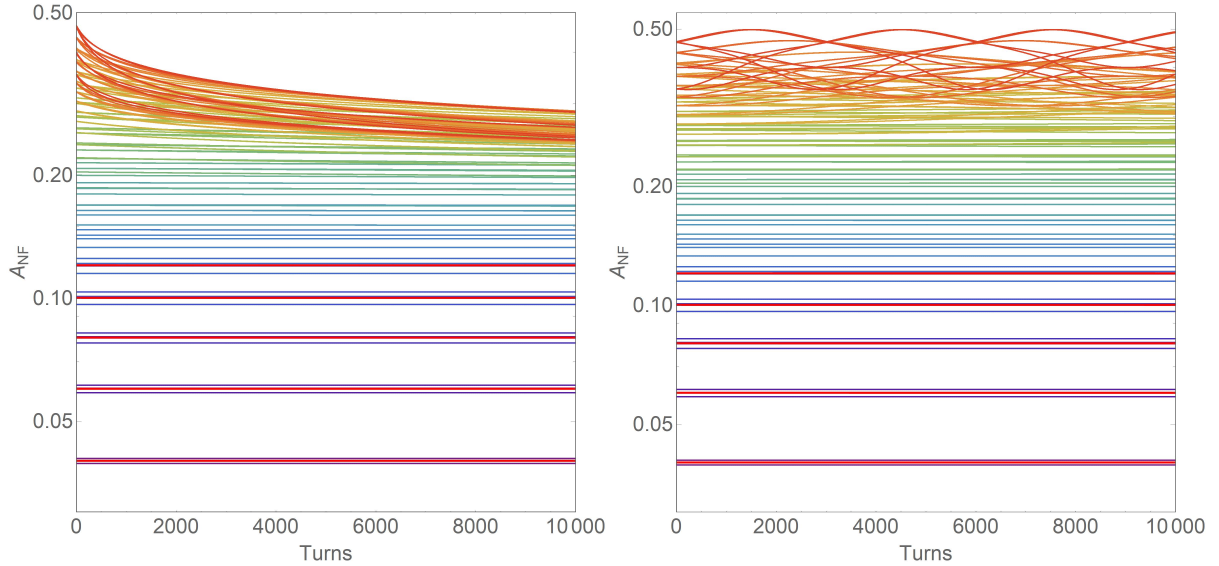


Figure 14: Cases COSY_CO7 (left) and COSY_CO7_TY0 (right) for the cell defined as the 45° degree electrostatic spherical deflector of radius 1 m. The normal form horizontal transverse amplitude A_{NF} [$\text{m}^{1/2}$] versus the number of turns. The initial normal form coordinates of the particles were $(x_{\text{NF}}, a_{\text{NF}}) = (0.02 \text{ m}^{1/2}, 0) \cdot j$ for $j = 2, 3, \dots, 20$. The logarithmic slopes of A_{NF} for the innermost five particles are -5.46×10^{-9} , -8.38×10^{-9} , -1.20×10^{-8} , -1.90×10^{-8} , -3.83×10^{-8} (left) and -5.46×10^{-9} , -8.30×10^{-9} , -1.12×10^{-8} , -1.42×10^{-8} , -1.72×10^{-8} (right).

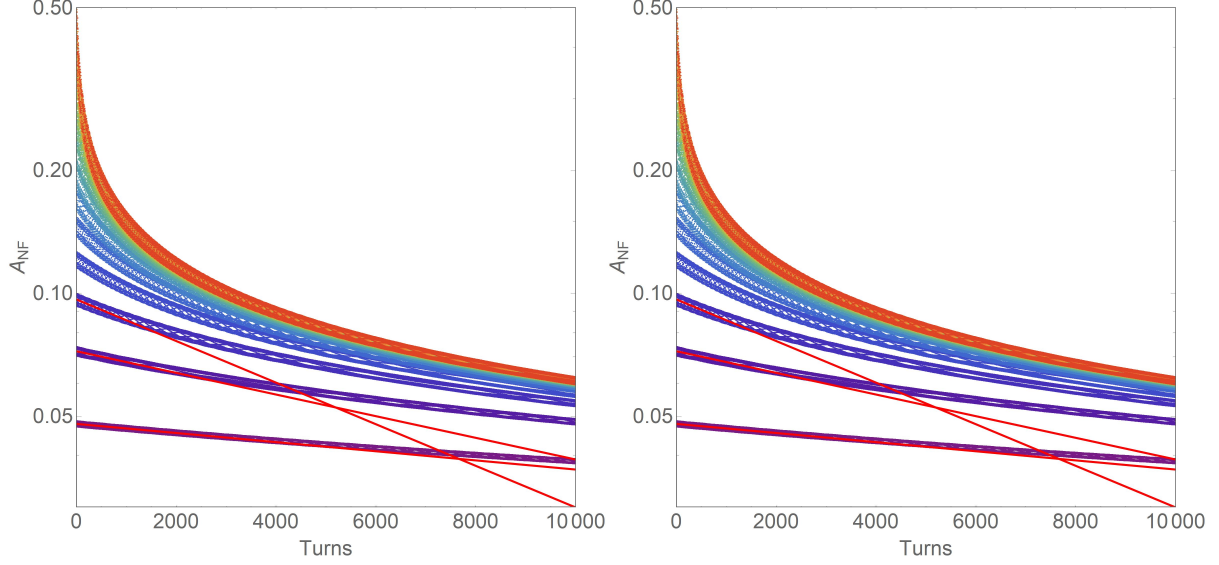


Figure 15: Cases EDABRT (left) and COSY (right) for the cell defined as the 45° degree electrostatic cylindrical deflector of radius 1 m. The normal form horizontal transverse amplitude A_{NF} [$\text{m}^{1/2}$] versus the number of turns. The initial normal form coordinates of the particles were $(x_{\text{NF}}, a_{\text{NF}}) = (2.38 \times 10^{-2} \text{ m}^{1/2}, 0) \cdot j$ for $j = 2, 3, \dots, 20$. The logarithmic slopes of A_{NF} for the innermost three particles are -2.57×10^{-5} , -6.10×10^{-5} , and -1.17×10^{-4} (both left and right).

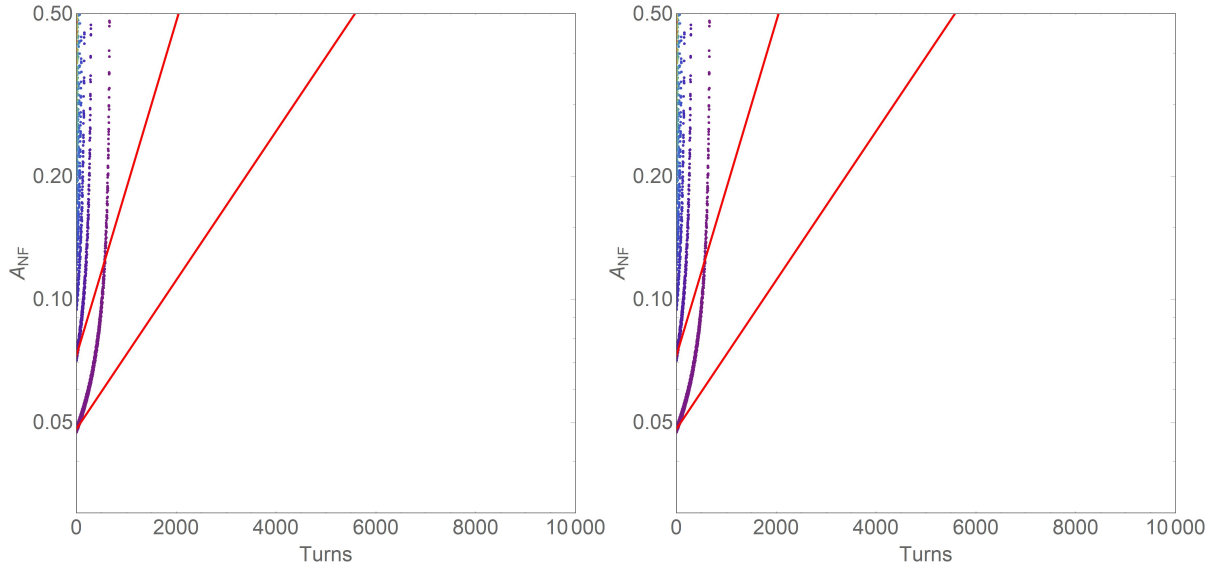


Figure 16: Cases LEGACY1965 (left) and GIOS (right) for the cell defined as the 45° degree electrostatic cylindrical deflector of radius 1 m. For every plotted point, scaling and descaling for a hard edge fringe field was performed for the initial coordinates in the first turn and the final coordinates in the last turn, respectively. The normal form horizontal transverse amplitude A_{NF} [$\text{m}^{1/2}$] versus the number of turns. The initial normal form coordinates of the particles were $(x_{\text{NF}}, a_{\text{NF}}) = (2.38 \times 10^{-2} \text{ m}^{1/2}, 0) \cdot j$ for $j = 2, 3, \dots, 20$. The logarithmic slopes of A_{NF} for the innermost two particles are 4.20×10^{-4} and 9.42×10^{-4} (both left and right).

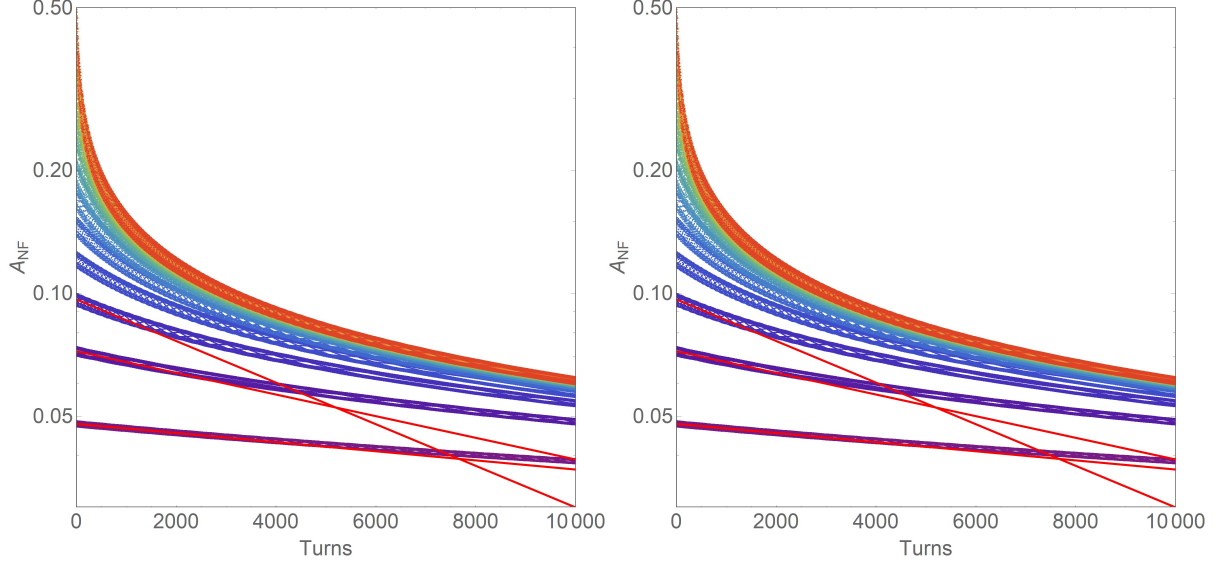


Figure 17: Cases LEGACY1965_Mod (left) and EDABRT (right) for the cell defined as the 45° degree electrostatic cylindrical deflector of radius 1 m. The normal form horizontal transverse amplitude A_{NF} [$\text{m}^{1/2}$] versus the number of turns. The initial normal form coordinates of the particles were $(x_{\text{NF}}, a_{\text{NF}}) = (2.38 \times 10^{-2} \text{ m}^{1/2}, 0) \cdot j$ for $j = 2, 3, \dots, 20$. The logarithmic slopes of A_{NF} for the innermost three particles are -2.57×10^{-5} , -6.10×10^{-5} , and -1.17×10^{-4} (both left and right).

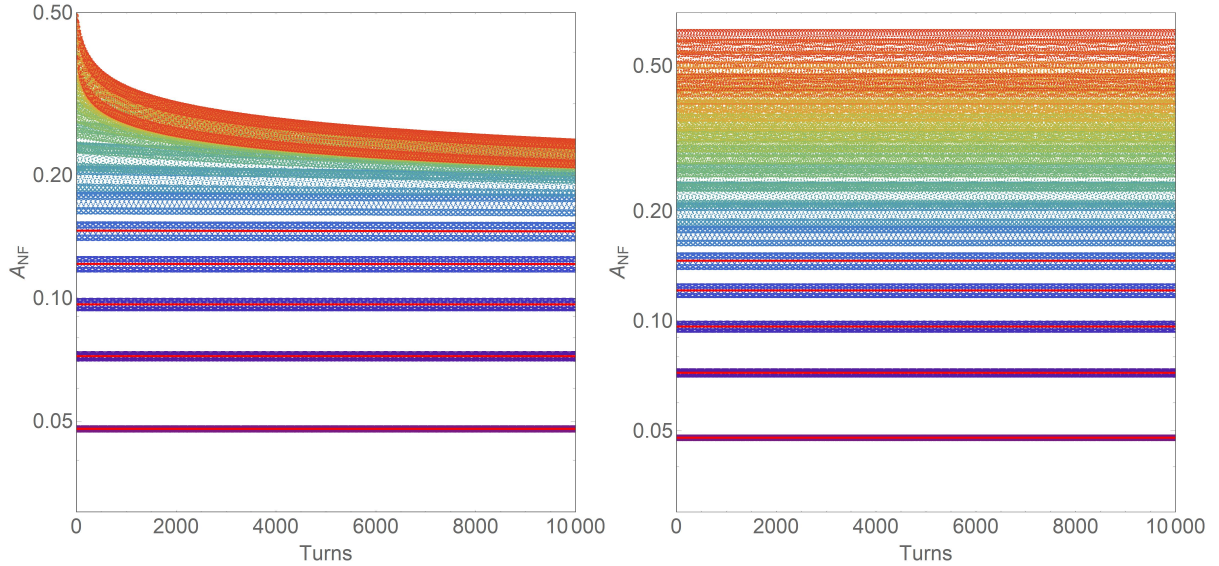


Figure 18: Cases COSY_CO7 (left) and COSY_CO7_TY0 (right) for the cell defined as the 45° degree electrostatic cylindrical deflector of radius 1 m. The normal form horizontal transverse amplitude A_{NF} [$\text{m}^{1/2}$] versus the number of turns. The initial normal form coordinates of the particles were $(x_{\text{NF}}, a_{\text{NF}}) = (2.38 \times 10^{-2} \text{ m}^{1/2}, 0) \cdot j$ for $j = 2, 3, \dots, 20$. The logarithmic slopes of A_{NF} for the innermost five particles are -9.25×10^{-9} , -2.18×10^{-8} , -2.87×10^{-8} , -9.06×10^{-8} , -3.74×10^{-7} (left) and -9.20×10^{-9} , -2.05×10^{-8} , -1.57×10^{-8} , -1.01×10^{-8} , -1.53×10^{-8} (right).

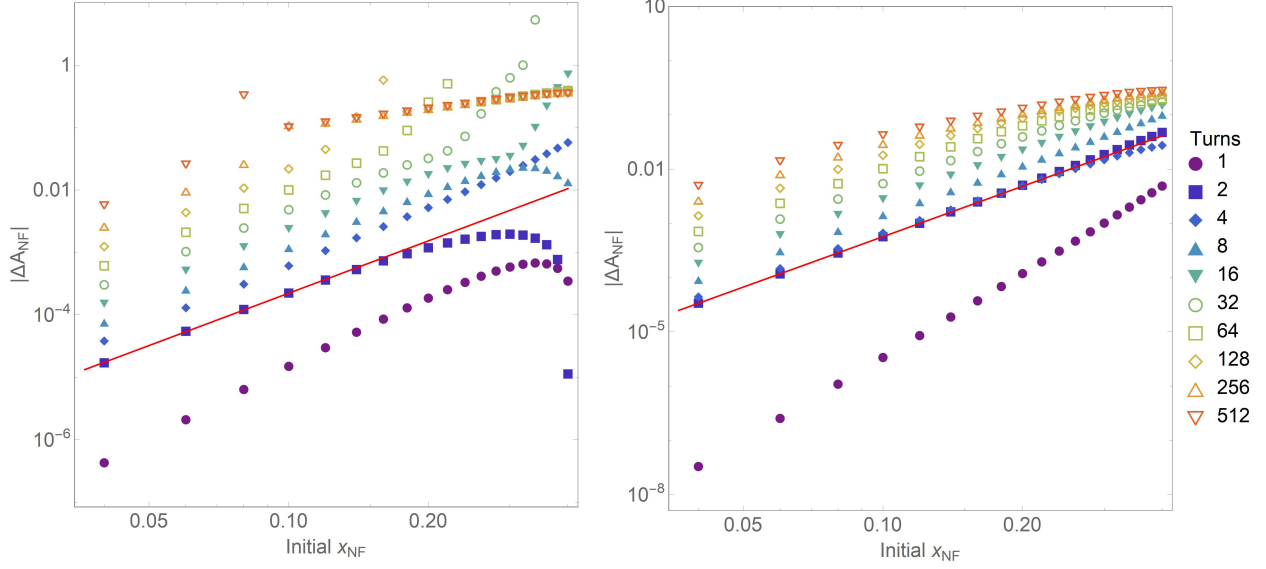


Figure 19: Cases LEGACY1965 (left) and LEGACY1965_Mod (right) for the cell as the 45° degree electrostatic spherical deflector of radius 1 m. Absolute values $|\Delta A_{\text{NF}}|$ of errors in the normal form horizontal transverse amplitude A_{NF} versus the initial normal form coordinates $(x_{\text{NF}}, 0)$ are shown for 2^j tracked turns, where $j = 0, 1, \dots, 9$. For every plotted point of Case LEGACY1965, scaling and descaling for a hard edge fringe field was performed for the initial coordinates in the first turn and final coordinates in the last turn, respectively. The error slopes are plotted for the second turn and are 2.78 for Case LEGACY1965 and 3.09 for Case LEGACY1965_Mod, considering that the first turn error slopes appears to be outliers. The units of normal form coordinates are $\text{m}^{1/2}$. The initial normal form coordinates of the particles were $(x_{\text{NF}}, a_{\text{NF}}) = (0.02 \text{ m}^{1/2}, 0) \cdot j$ for $j = 2, 3, \dots, 20$.

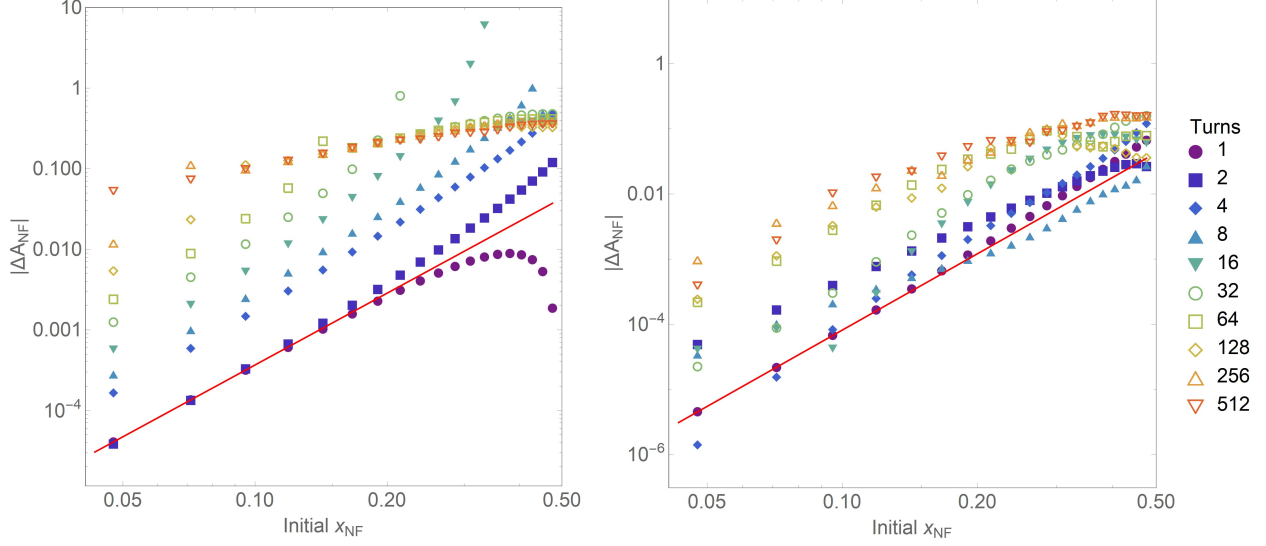


Figure 20: Cases LEGACY1965 (left) and LEGACY1965_Mod (right) for the cell as the 45° degree electrostatic cylindrical deflector of radius 1 m. Absolute values $|\Delta A_{\text{NF}}|$ of errors in the normal form horizontal transverse amplitude A_{NF} versus the initial normal form coordinates $(x_{\text{NF}}, 0)$ are shown for 2^j tracked turns, where $j = 0, 2, \dots, 9$. For every plotted point of Case LEGACY1965, scaling and descaling for a hard edge fringe field was performed for the initial coordinates in the first turn and final coordinates in the last turn, respectively. The error slopes are plotted for the first turn and are 2.96 for Case LEGACY1965 and 3.90 for Case LEGACY1965_Mod. The units of normal form coordinates are $\text{m}^{1/2}$. The initial normal form coordinates of the particles were $(x_{\text{NF}}, a_{\text{NF}}) = (2.38 \times 10^{-2} \text{ m}^{1/2}, 0) \cdot j$ for $j = 2, 3, \dots, 20$.

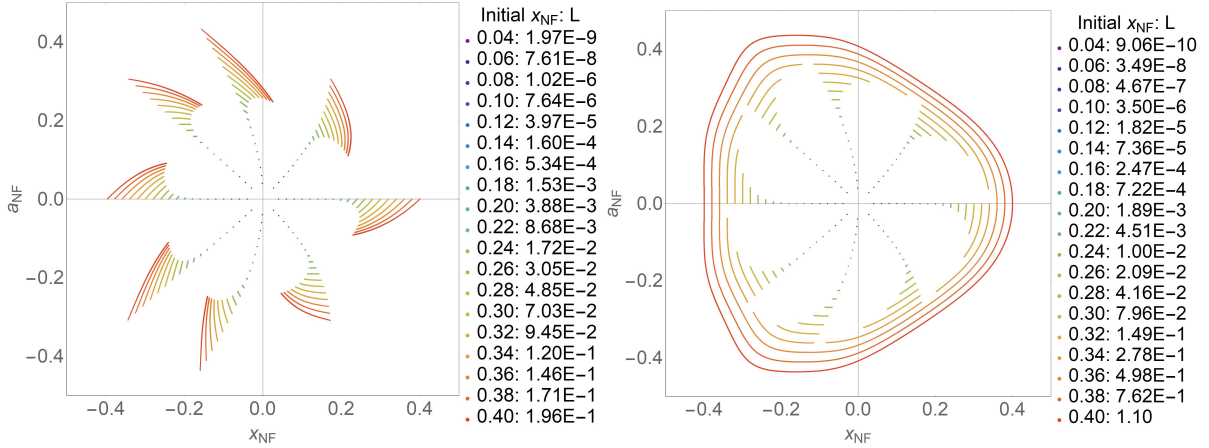


Figure 21: Cases COSY_CO7 (left) and COSY_CO7_TY0 (right) for the electrostatic spherical deflector. Tracking picture in the horizontal transverse plane in normal form coordinates $(x_{\text{NF}}, a_{\text{NF}})$ for particles launched with initial normal form coordinates $(x_{\text{NF}}, a_{\text{NF}}) = (0.02 \text{ m}^{1/2}, 0) \cdot j$ for $j = 2, 3, \dots, 20$ through an electrostatic spherical deflector of radius 1 m and central angle 45° . Particles were tracked for 10000 turns. For each initial x_{NF} , the plot legend indicates the length L of the arc formed due to truncation errors by particle coordinates in every 8th turn, starting from turn 0. These arcs begin at initial coordinates with $x_{\text{NF}} > 0$ and $a_{\text{NF}} = 0$. The units of normal form coordinates are $\text{m}^{1/2}$.

5 Conclusion

We derived analytic formulas for the first and second order aberrations of an electrostatic deflector in the horizontal transverse x - a plane using an order-by-order perturbation method, and we listed them in eqns. 44–45. The derivations were performed in *COSY INFINITY*'s Frenet–Serret beamline coordinate system.

We implemented a C program called `edabrt` that uses these analytic formulas to calculate the first and second order aberrations for an electrostatic deflector using eqns. 44–45, as well as a *COSY INFINITY* program `ESCP010AIEP.FOX` to compute all test cases considered in this work. We calculated the aberrations for the test cases of an electrostatic spherical deflector and an electrostatic cylindrical deflector using eqns. 44–45, and we compared the results with *COSY INFINITY*'s elements `ESP` and `ECL`, respectively. The comparison shows excellent agreement between our aberration formulas and *COSY INFINITY*'s numerical DA calculation².

Comparison of the first and second order aberrations calculation using analytic formulas from eqns. 44–45 and the code *COSY INFINITY* with analytic formulas from Wollnik's paper (Wollnik, 1965) and the code *GIOS*, which uses the aberration formulas from Wollnik's paper, shows significant discrepancies in the latter two. Valetov (in this volume) investigated the source of these discrepancies and found that while the aberration formulas from Wollnik's paper correctly account for motion within the main field, they do not account for any fringe field effects. On the other hand, the aberration formulas derived by us in Sec. 3 are valid both within the main field (without considering any fringe field) and with a hard edge fringe field because of the definition of *COSY INFINITY*'s beamline coordinates. Accordingly, Valetov (in this volume) modified the aberration formulas from Wollnik's paper by scaling the initial and final particle inclinations to account for a hard edge fringe field, and here we found a full agreement of these modified aberration formulas with eqns. 44–45 and *COSY INFINITY*.

Deviations from the conditions of symplecticity g_1 , g_2 , and g_3 were nearly at machine precision for *COSY INFINITY*'s built-in electrostatic deflector elements, analytic aberration formulas from eqns. 44–45, and formulas from Wollnik's paper modified by Valetov (in this volume) to account for a hard edge fringe field. In particular, deviations from the conditions of symplecticity g_1 , g_2 , and g_3 in *COSY INFINITY* calculations were all of the order $\sim 3 \times 10^{-16}$. For aberrations of eqns. 44–45, these deviations ranged from 0 to $\sim 10^{-16}$. Aberration formulas from Wollnik's paper, after our modifications for a hard edge fringe field, also had deviations from the conditions of symplecticity from 0 to $\sim 10^{-16}$. On the other hand, the deviations from second order conditions of symplecticity g_2 and g_3 were substantial for *GIOS* and the original aberration formulas from Wollnik's paper.

The comparison cross-validates the analytic aberration formulas derived in this work, *COSY INFINITY*'s built-in electrostatic deflector elements, and aberration formulas from Wollnik's paper modified by us to account for a hard edge fringe field. It also illustrates the high accuracy of numerical DA integration performed in *COSY INFINITY* for calculation of transfer maps of particle optical elements. The electrostatic deflector aberrations presented in this work agree with electrostatic deflector transfer maps computed by Valetov et al. (in print) in polar laboratory coordinates.

6 Electronic Supplementary Material

The C program `edabrt` and the *COSY INFINITY* code `ESCP010AIEP.FOX` to compute all test cases considered in this text are provided via the Reprint Server of Michigan State University's Center for Beam Theory and Dynamical Systems (Valetov & Berz, 2019). This supplementary material can be also found by searching online for “ESCP010AIEP”.

²We also compared first and second order aberrations computed by `edabrt` and *COSY INFINITY* for electrostatic deflectors other than spherical and cylindrical, and similarly found excellent agreement. We did not include those additional results in this work.

7 Acknowledgment

This work was supported by the U.S. Department of Energy under Contract No. DE-FG02-08ER41546.

References

- Anastassopoulos, D. et al. (2008). *AGS proposal: Search for a permanent electric dipole moment of the deuteron nucleus at the 10^{-29} e-cm level*. Brookhaven National Laboratory, Upton, NY. Retrieved from https://www.bnl.gov/edm/files/pdf/deuteron_proposal_080423_final.pdf
- Berz, M. (1999). *Modern map methods in particle beam physics*. San Diego, CA: Academic Press.
- Berz, M., & Makino, K. (2017). *COSY INFINITY 10.0 beam physics manual*. Department of Physics and Astronomy, Michigan State University, East Lansing, MI 48824.
- Berz, M., Makino, K., & Wan, W. (2014). *An introduction to beam physics*. London: CRC Press.
- Deriglazov, A. (2017). *Classical mechanics: Hamiltonian and Lagrangian formalism* (2nd). doi:10.1007/978-3-319-44147-4
- Dorf, R. C., & Bishop, R. H. (2017). *Modern control systems* (13th). Harlow, England: Pearson.
- Erdélyi, B., & Berz, M. (2001). Optimal symplectic approximation of Hamiltonian flows. *Physical Review Letters*, 87(11), 114302–114302. doi:10.1103/PhysRevLett.87.114302
- Graham, R. L., Knuth, D. E., & Patashnik, O. (1994). *Concrete mathematics: A foundation for computer science* (2nd). Reading, MA: Addison–Wesley.
- Grimshaw, R. (1990). *Nonlinear ordinary differential equations*. Boca Raton, FL: Blackwell Scientific Publications.
- Hunter, J. K., & Nachtergaele, B. (2001). *Applied analysis*. doi:10.1142/4319
- Kühnel, W. (2015). *Differential geometry: Curves, surfaces, manifolds* (3rd). Providence, RI: American Mathematical Society.
- Lebedev, V., & Ostiguy, J.-F. (n.d.). Optimx: A program for accelerator optics [Coordinate system]. Retrieved from <http://home.fnal.gov/%7Eostiguy/OptiM/>
- Lee, S. Y. (2012). *Accelerator physics* (3rd). doi:10.1142/8335
- Makino, K., & Berz, M. (2006). COSY INFINITY version 9. *Nucl. Instr. Meth. Phys. Res. A*, 558(1), 346–350. doi:10.1016/j.nima.2005.11.109
- Makino, K., & Berz, M. (2015). Dynamics in electrostatic repetitive systems via high-order transfer maps. *Microsc. Microanal.*, 21(S4), 36–43. doi:10.1017/S1431927615013100
- McCleary, J. (2013). *Geometry from a differentiable viewpoint* (2nd). doi:10.1017/CBO9781139022248
- Russenschuck, S. (2010). *Field computation for accelerator magnets: Analytical and numerical methods for electromagnetic design and optimization*. doi:10.1002/9783527635467
- Sagan, D. (2018). *The Bmad reference manual (rev. 31.10)*. Wilson Laboratory, Cornell University, Ithaca, NY. Retrieved from <https://www.classe.cornell.edu/bmad/manual.html>
- Senichev, Y., Andrianov, S., Berz, M., Chekmenev, S., Ivanov, A., Lehrach, A., . . . Valetov, E. (2015). Quasi-frozen spin method for EDM deuteron search. In S. Henderson, T. Satoga, & V. R. Schaa (Eds.), *Proceedings, 6th International Particle Accelerator Conference (IPAC 2015): Richmond, Virginia, USA, May 3-8, 2015* (MOPWA044). Geneva, Switzerland: JACoW. Retrieved from <http://accelconf.web.cern.ch/AccelConf/IPAC2015/papers/mopwa044.pdf>
- Struik, D. J. (1961). *Lectures on classical differential geometry* (2nd). Reading, MA: Addison-Wesley Pub. Co.
- Stupakov, G., & Penn, G. (2018). *Classical mechanics and electromagnetism in accelerator physics*. doi:10.1007/978-3-319-90188-6
- Talman, R. (2007). *Geometric mechanics: Toward a unification of classical physics* (2nd, revised and enlarged). Weinheim, Germany: Wiley-VCH.
- Teschl, G. (2012). *Ordinary differential equations and dynamical systems*. Providence, RI: American Mathematical Society.

- Valetov, E. (in this volume). Analysis and fringe field scaling of a legacy set of electrostatic deflector aberration formulas. *Advances in Imaging and Electron Physics*.
- Valetov, E. (2017). *Field modeling, symplectic tracking, and spin decoherence for EDM and Muon $g-2$ lattices*. Michigan State University. Fermilab report FERMILAB-THESIS-2017-21. East Lansing, MI.
- Valetov, E., & Berz, M. (2019). Derivation, cross-validation, and comparison of analytic formulas for electrostatic deflector aberrations (supplementary electronic resources). Retrieved from <https://bt.pa.msu.edu/cgi-bin/display.pl?name=ESCPO10AIEP>
- Valetov, E., Berz, M., & Makino, K. (in print). Validation of transfer map calculation for electrostatic deflectors in the code *COSY INFINITY*. *Int. J. Mod. Phys. A*.
- Wollnik, H. (1965). Second order approximation of the three-dimensional trajectories of charged particles in deflecting electrostatic and magnetic fields. *Nucl. Instrum. Methods*, *34*, 213–221. doi:10.1016/0029-554X(65)90297-1
- Wollnik, H., & Berz, M. (1985). Relations between elements of transfer matrices due to the condition of symplecticity. *Nucl. Instr. Meth. Phys. Res. A*, *238*(1), 127–140.

A Derivation of the ODEs of Motion in Beamline Coordinates

In the following, we will derive the ODEs of motion of a charged particle in *COSY INFINITY*'s beamline coordinate system from the well-known Lagrangian of a charged particle in electromagnetic field. We will begin by describing the Frenet–Serret framework, deriving the Frenet–Serret theorem, and noting the relevant beam physics conventions.

A.1 Frenet–Serret Coordinate System

Consider an ensemble of charged particles moving through the electromagnetic field, with one particle designated as the reference particle. The reference orbit of the system is the trajectory of the reference particle. The following two coordinate systems will be used: (1) a Cartesian laboratory coordinate system (LCS) and (2) a Frenet–Serret coordinate system associated with the reference orbit.

Let $\vec{r}_0(t)$ denote the position of the reference particle at time t in the Cartesian LCS. We parameterize the reference orbit by arc length $s(t)$, which is the distance traveled along the reference orbit by the reference particle between times t_0 and t :

$$s(t) = \int_{t_0}^t \left\| \dot{\vec{r}}_0(t) \right\| dt, \quad (64)$$

where $\dot{\vec{r}}_0(t)$ is the velocity of the reference particle at time t , also denoted as $\vec{v}_0(t)$. The subscript 0 denotes the reference particle. Here and in the following, we use Newton's dot notation (e.g. $\dot{\vec{r}}(t)$) for the time derivative, whereas Lagrange's prime notation (e.g. $\vec{r}'(s)$) is used for the derivative by arc length s .

We denote the basis vectors of the Cartesian LCS as

$$(\vec{e}_1, \vec{e}_2, \vec{e}_3), \quad (65)$$

with basis vector \vec{e}_3 pointing upward vertically and basis vectors \vec{e}_1 and \vec{e}_2 lying in the horizontal plane.

For the following, we note that

$$\begin{aligned} \|\vec{r}'_0(s)\| &= \left\| \frac{dt}{ds} \frac{d}{dt} \vec{r}_0(t) \right\| = \\ &= \left\| \frac{\dot{\vec{r}}_0(t)}{\|\dot{\vec{r}}_0(t)\|} \right\| = \\ &= 1. \end{aligned} \quad (66)$$

The Frenet–Serret frame is orthonormal and is constructed from the following arc length–dependent basis vectors (Kühnel, 2015; Russenschuck, 2010; Struik, 1961):

1. the tangent unit vector

$$\vec{e}_s(s) = \vec{r}'_0(s) \quad (67)$$

2. the normal unit vector

$$\begin{aligned} \vec{e}_x(s) &= \frac{\vec{e}'_s(s)}{\|\vec{e}'_s(s)\|} = \\ &= \frac{\vec{r}''_0(s)}{\|\vec{r}''_0(s)\|}; \text{ and} \end{aligned} \quad (68)$$

3. the binormal unit vector

$$\vec{e}_y(s) = \vec{e}_s(s) \times \vec{e}_x(s). \quad (69)$$

A.1.1 Basis and Coordinate Transformations

The basis vectors of the LCS can be expressed in terms of the basis vectors of the Frenet–Serret coordinate system as (Berz, 1999)

$$\begin{pmatrix} \vec{e}_1 \\ \vec{e}_2 \\ \vec{e}_3 \end{pmatrix} = \hat{O}(s) \begin{pmatrix} \vec{e}_s(s) \\ \vec{e}_x(s) \\ \vec{e}_y(s) \end{pmatrix}, \quad (70)$$

where

$$\hat{O}(s) = \begin{pmatrix} (\vec{e}_s(s) \cdot \vec{e}_1) & (\vec{e}_x(s) \cdot \vec{e}_1) & (\vec{e}_y(s) \cdot \vec{e}_1) \\ (\vec{e}_s(s) \cdot \vec{e}_2) & (\vec{e}_x(s) \cdot \vec{e}_2) & (\vec{e}_y(s) \cdot \vec{e}_2) \\ (\vec{e}_s(s) \cdot \vec{e}_3) & (\vec{e}_x(s) \cdot \vec{e}_3) & (\vec{e}_y(s) \cdot \vec{e}_3) \end{pmatrix}. \quad (71)$$

Because the columns of the matrix $\hat{O}(s)$ are an orthonormal basis, namely the basis of the Frenet–Serret coordinate system, the matrix $\hat{O}(s)$ is orthogonal. That is, $\hat{O}(s) \cdot \hat{O}^T(s) = \hat{I}$, where \hat{I} is the identity matrix. This gives the inverse coordinate transformation as

$$\begin{pmatrix} \vec{e}_s(s) \\ \vec{e}_x(s) \\ \vec{e}_y(s) \end{pmatrix} = \hat{O}^T(s) \begin{pmatrix} \vec{e}_1 \\ \vec{e}_2 \\ \vec{e}_3 \end{pmatrix}. \quad (72)$$

Consider a three-dimensional vector \vec{c} , which may be, e.g., velocity or the vector potential. Expressing it via its components in the LCS and the Frenet–Serret coordinate system as

$$\vec{c} = (c_1, c_2, c_3) \begin{pmatrix} \vec{e}_1 \\ \vec{e}_2 \\ \vec{e}_3 \end{pmatrix} = (c_s(s), c_x(s), c_y(s)) \begin{pmatrix} \vec{e}_s(s) \\ \vec{e}_x(s) \\ \vec{e}_y(s) \end{pmatrix} \quad (73)$$

and applying eq. 70, we obtain

$$\left[(c_1, c_2, c_3) \hat{O}(s) - (c_s(s), c_x(s), c_y(s)) \right] \begin{pmatrix} \vec{e}_s(s) \\ \vec{e}_x(s) \\ \vec{e}_y(s) \end{pmatrix} = 0, \quad (74)$$

from where (Berz, 1999)

$$\begin{pmatrix} \vec{c}_s(s) \\ \vec{c}_x(s) \\ \vec{c}_y(s) \end{pmatrix} (s) = \hat{O}^T(s) \begin{pmatrix} \vec{c}_1 \\ \vec{c}_2 \\ \vec{c}_3 \end{pmatrix}. \quad (75)$$

A.1.2 Frenet–Serret Theorem

Derivative of the tangent unit vector by arc length Taking the derivative of the tangent unit vector $\vec{e}_s(s)$ by s , by eq. 68, we have that

$$\begin{aligned} \frac{d\vec{e}_s(s)}{ds} &= \frac{d\vec{r}'_0(s)}{ds} = \\ &= h(s) \vec{e}_x(s), \end{aligned} \quad (76)$$

where the proportionality coefficient

$$h(s) = \|\vec{r}''_0(s)\| \quad (77)$$

is called the curvature. We remark that the instantaneous curvature radius of the reference orbit is

$$\begin{aligned} R(s) &= h^{-1}(s) = \\ &= \|\vec{r}''_0(s)\|^{-1}. \end{aligned} \quad (78)$$

Derivative of the binormal unit vector by arc length By the definition of the binormal unit vector $\vec{e}_y(s)$ from eq. 69, we get

$$\begin{aligned}
\frac{d\vec{e}_y(s)}{ds} &= \frac{d}{ds} (\vec{e}_s(s) \times \vec{e}_x(s)) = \\
&= \frac{d}{ds} \left(\vec{r}'_0(s) \times \frac{\vec{r}''_0(s)}{\|\vec{r}''_0(s)\|} \right) = \\
&= \vec{r}''_0(s) \times \frac{\vec{r}'_0(s)}{\|\vec{r}'_0(s)\|} + \vec{r}'_0(s) \times \frac{d}{ds} \left(\frac{\vec{r}''_0(s)}{\|\vec{r}''_0(s)\|} \right) = \\
&= \vec{e}_s(s) \times \frac{d}{ds} \vec{e}_x(s).
\end{aligned} \tag{79}$$

Both the tangent unit vector $\vec{e}_s(s)$ and the derivative of the normal unit vector $\vec{e}_x(s)$ by s being perpendicular to the normal unit vector $\vec{e}_x(s)$, we find that $d\vec{e}_y(s)/ds$ is proportional to $\vec{e}_x(s)$:

$$\frac{d\vec{e}_y(s)}{ds} = -\tau(s) \vec{e}_x(s) \tag{80}$$

with a proportionality coefficient

$$\tau(s) = -\vec{e}_x(s) \cdot \frac{d\vec{e}_y(s)}{ds} \tag{81}$$

that defines torsion.

Derivative of the normal unit vector by arc length Considering the transformations of coordinates in eqns. 70 and 72, we obtain

$$\begin{aligned}
\frac{d}{ds} \begin{pmatrix} \vec{e}_s \\ \vec{e}_x \\ \vec{e}_y \end{pmatrix} (s) &= \frac{d}{ds} \hat{O}^T(s) \begin{pmatrix} \vec{e}_1 \\ \vec{e}_2 \\ \vec{e}_3 \end{pmatrix} = \\
&= \hat{Q}(s) \begin{pmatrix} \vec{e}_s \\ \vec{e}_x \\ \vec{e}_y \end{pmatrix},
\end{aligned} \tag{82}$$

where the matrix $\hat{Q}(s)$ is defined as

$$\hat{Q}(s) = \frac{d\hat{O}^T(s)}{ds} \hat{O}(s). \tag{83}$$

Because the matrix $\hat{O}(s)$ is orthogonal, we have $\hat{O}^T(s) \hat{O}(s) = \hat{I}$, and (Berz, 1999)

$$\begin{aligned}
\frac{d}{ds} \left(\hat{O}^T(s) \hat{O}(s) \right) &= \frac{d\hat{O}^T(s)}{ds} \hat{O}(s) + \hat{O}^T(s) \frac{d\hat{O}(s)}{ds} = \\
&= \hat{Q}(s) + \hat{Q}^T(s) = \\
&= 0,
\end{aligned} \tag{84}$$

which means that the matrix $\hat{Q}(s)$ is skew-symmetric. (Skew-symmetric matrices are also called antisymmetric.) Because of this skew symmetry property, from eqns. 76 and 80, it follows (compare with Kühnel (2015), Russenschuck (2010), Struik (1961)) that

$$\hat{Q}(s) = \begin{pmatrix} 0 & h(s) & 0 \\ -h(s) & 0 & \tau(s) \\ 0 & -\tau(s) & 0 \end{pmatrix}. \tag{85}$$

Frenet–Serret Theorem The derivation of eq. 85 performed above constitutes a proof of the Frenet–Serret theorem in application to the reference orbit. The Frenet–Serret theorem states (McCleary, 2013) that

$$\frac{d}{ds} \begin{pmatrix} \vec{e}_s \\ \vec{e}_x \\ \vec{e}_y \end{pmatrix} (s) = \begin{pmatrix} 0 & h(s) & 0 \\ -h(s) & 0 & \tau(s) \\ 0 & -\tau(s) & 0 \end{pmatrix} \cdot \begin{pmatrix} \vec{e}_s \\ \vec{e}_x \\ \vec{e}_y \end{pmatrix} (s), \quad (86)$$

where $h(s)$ is curvature

$$h(s) = \left\| \frac{d\vec{e}_s(s)}{ds} \right\| \quad (87)$$

and $\tau(s)$ is torsion

$$\tau(s) = -\vec{e}_x(s) \cdot \frac{d\vec{e}_y(s)}{ds}. \quad (88)$$

A.1.3 Beam Physics Conventions

In view of the conventions and specifics of beam physics, we

1. assume that the reference orbit lies in the horizontal plane (Berz (1999), Stupakov and Penn (2018); also see Russenschuck (2010), Sagan (2018));
2. traverse the lattice in the clockwise direction (Berz & Makino, 2017; Lebedev & Ostiguy, n.d. Sagan, 2018); and
3. replace the vector $\vec{e}_x(s)$ by its inverse (see, e.g., Berz et al. (2014), Lee (2012), Sagan (2018), and compare with the generic definition in eq. 68), which means that now

$$\vec{e}_x(s) = -\frac{\vec{r}_0''(s)}{\|\vec{r}_0''(s)\|} \quad (89)$$

and the beam physics version of the Frenet equations are formulated (compare with matrix \hat{T} of Berz (1999)) as

$$\frac{d}{ds} \begin{pmatrix} \vec{e}_s \\ \vec{e}_x \\ \vec{e}_y \end{pmatrix} (s) = \begin{pmatrix} 0 & -h(s) & 0 \\ h(s) & 0 & -\tau(s) \\ 0 & \tau(s) & 0 \end{pmatrix} \cdot \begin{pmatrix} \vec{e}_s \\ \vec{e}_x \\ \vec{e}_y \end{pmatrix} (s). \quad (90)$$

Hence, we also find that basis vectors $\vec{e}_s(s)$ and $\vec{e}_x(s)$ lie in the horizontal plane, while the binormal unit vector $\vec{e}_y(s)$ points upward vertically and is equal to \vec{e}_3 . Because $\vec{e}_y(s)$ is constant, it follows from eq. 90 that torsion $\tau(s)$ is zero.

A.1.4 Velocity in the Frenet–Serret Coordinate System

For velocity $\vec{v}(s)$ of an off-reference orbit particle with coordinates (x, y) in the Frenet–Serret coordinate system, applying eqns. 90 and 67, we obtain

$$\begin{aligned} \vec{v}(s) &= \frac{d}{ds} \vec{r}(s) = \\ &= \frac{d}{ds} (\vec{r}_0(s) + x\vec{e}_x(s) + y\vec{e}_y(s)) = \\ &= (1 + hx) \vec{e}_s(s) + v_x(s) \vec{e}_x(s) + v_y \vec{e}_y(s). \end{aligned} \quad (91)$$

From eq. 91, we also have

$$v^2(s) = (1 + hx)^2 + v_x^2(s) + v_y^2(s). \quad (92)$$

From here on forward, we omit the argument s for simplicity.

A.2 Lagrangian of a Charged Particle

We consider a particle with mass m and charge Ze moving with velocity $\vec{v} = \dot{\vec{r}}$ through an electromagnetic field with vector potential \vec{A} and scalar potential φ , where e is the elementary charge. In the Cartesian LCS, the particle has the well-known relativistic Lagrangian (Berz, 1999; Deriglazov, 2017; Talman, 2007)

$$L^{\text{ct}}(\vec{r}, \vec{v}, t) = -mc^2 \sqrt{1 - \frac{v^2}{c^2}} + Ze\vec{A}^{\text{ct}} \cdot \vec{v}^{\text{ct}} - Ze\varphi^{\text{ct}}, \quad (93)$$

where the subscript ct denotes the Cartesian LCS.

The Lagrangian action of the charged particle is

$$S[\vec{r}] = \int_{t_0}^t dt L^{\text{ct}}(\vec{r}, \dot{\vec{r}}, t). \quad (94)$$

Changing the independent variable from time t to arc length s (which is $s = h^{-1}\theta$ in case the reference trajectory has a constant curvature h with θ as the respective central angle) and thus also making t a dependent position variable, we obtain

$$\begin{aligned} S[\vec{r}] &= \int_{t_0}^t dt \left(-mc^2 \sqrt{1 - \frac{v^2}{c^2}} + Ze\vec{A}^{\text{ct}} \cdot \vec{v}^{\text{ct}} - Ze\varphi^{\text{ct}} \right) = \\ &= \int_{s_0}^s ds \frac{1}{\dot{s}} \left(-mc^2 \sqrt{1 - \frac{(v^s)^2}{c^2}} \dot{s}^2 + Ze\vec{A}^{\text{ct}} \cdot \vec{v}^{\text{ct},s} \dot{s} - Ze\varphi^{\text{ct}} \right), \end{aligned} \quad (95)$$

where the superscript s denotes arc length as the independent variable. This gives the Lagrangian of the charged particle in the Cartesian LCS with arc length s as the independent variable:

$$L^{\text{ct},s}(\vec{r}, \vec{v}^s, s) = \frac{1}{\dot{s}} \left(-mc^2 \sqrt{1 - \frac{(v^s)^2}{c^2}} \dot{s}^2 + Ze\vec{A}^{\text{ct}} \cdot \vec{v}^{\text{ct},s} \dot{s} - Ze\varphi^{\text{ct}} \right). \quad (96)$$

The scalar product of vectors is invariant under an orthogonal transformation, which is why

$$\vec{A}^{\text{ct}} \cdot \vec{v}^{\text{ct},s} = \vec{A}^{\text{C}} \cdot \vec{v}^{\text{C},s}, \quad (97)$$

where the superscript C refers to the Frenet–Serret coordinate system. A scalar field is also invariant under a coordinate transformation; in particular, $\varphi^{\text{ct}} = \varphi^{\text{C}}$ at every point in space.

Hence, eq. 96 in the Frenet–Serret coordinate system with arc length s as the independent variable is

$$L^{\text{C},s}(\vec{r}, \vec{v}^s, s) = \frac{1}{\dot{s}} \left(-mc^2 \sqrt{1 - \frac{(v^s)^2}{c^2}} \dot{s}^2 + Ze\vec{A}^{\text{C}} \cdot \vec{v}^{\text{C},s} \dot{s} - Ze\varphi^{\text{C}} \right). \quad (98)$$

In the non-relativistic limit $\gamma \rightarrow 1$, this Lagrangian takes the form

$$L^{\text{C},s}(\vec{r}, \vec{v}^s, s) = \frac{1}{\dot{s}} \left(\frac{m(v^s)^2}{2} \dot{s}^2 + Ze\vec{A}^{\text{C}} \cdot \vec{v}^{\text{C},s} \dot{s} - Ze\varphi^{\text{C}} \right). \quad (99)$$

A.3 Derivation of the Equations of Motion

In the following derivation of the equations of motion of the charged particle, we will operate in the Frenet–Serret coordinate system with arc length s as the independent variable.

Generalized and kinematic momenta First, we obtain the generalized momenta (P_x, P_y) canonically conjugate to the coordinates (x, y) from the Lagrangian $L = L^{C,s}(\vec{r}, \vec{v}^s, s)$ specified in eq. 98:

$$\begin{aligned} P_x &= \frac{\partial L}{\partial x'} = \\ &= \frac{1}{\dot{s}} \left[mc^2 \left(1 - \frac{(v^s)^2}{c^2} \dot{s}^2 \right)^{-\frac{1}{2}} v_x^{C,s} \frac{\dot{s}^2}{c^2} + ZeA_x^C \dot{s} \right] = \\ &= \gamma m v_x^{C,s} \dot{s} + ZeA_x^C \end{aligned} \quad (100)$$

and, similarly,

$$P_y = \gamma m v_y^{ct,s} \dot{s} + ZeA_y^{ct}. \quad (101)$$

Accordingly, the kinematic momenta are, considering eq. 91,

$$\begin{aligned} \begin{pmatrix} p_s \\ p_x \\ p_y \end{pmatrix} &= \gamma m \frac{d}{ds} \vec{r}(s) \dot{s} = \\ &= \gamma m \begin{pmatrix} 1 + hx \\ v_x^s \\ v_y^s \end{pmatrix} \dot{s}. \end{aligned} \quad (102)$$

Euler–Lagrange equation By the Euler–Lagrange equation, considering eqns. 100–102 and eq. 92, we have

$$\begin{aligned} \frac{d}{ds} \begin{pmatrix} P_x \\ P_y \end{pmatrix} &= \frac{d}{ds} \begin{pmatrix} p_x \\ p_y \end{pmatrix} + Ze \frac{d}{ds} \begin{pmatrix} A_x \\ A_y \end{pmatrix} = \\ &= \begin{pmatrix} \frac{\partial L}{\partial x} \\ \frac{\partial L}{\partial y} \end{pmatrix} = \\ &= \frac{1}{2\dot{s}} \gamma m \begin{pmatrix} \frac{\partial}{\partial x} \\ \frac{\partial}{\partial y} \end{pmatrix} (v^s)^2 \dot{s}^2 + \frac{1}{\dot{s}} Ze \begin{pmatrix} \frac{\partial}{\partial x} \\ \frac{\partial}{\partial y} \end{pmatrix} (\vec{A}^C \cdot \vec{v}^{C,s} \dot{s} - \varphi^C) = \\ &= \gamma m \begin{pmatrix} h(1+hx) \\ 0 \end{pmatrix} \dot{s} + Ze \begin{pmatrix} \frac{\partial}{\partial x} \\ \frac{\partial}{\partial y} \end{pmatrix} \left(\vec{A}^C \cdot \vec{v}^{C,s} - \frac{1}{\dot{s}} \varphi^C \right) = \\ &= \begin{pmatrix} hp_s \\ 0 \end{pmatrix} + Ze \begin{pmatrix} \frac{\partial}{\partial x} \\ \frac{\partial}{\partial y} \end{pmatrix} \left(\vec{A}^C \cdot \vec{v}^{C,s} - \frac{1}{\dot{s}} \varphi^C \right). \end{aligned} \quad (103)$$

Derivation of ODEs for scaled momenta (part 1) Instead of the kinematic momenta (p_x, p_y, p_s) , we will use scaled quantities

$$\begin{pmatrix} \zeta \\ a \\ b \end{pmatrix} = \frac{1}{p_0} \begin{pmatrix} p_s \\ p_x \\ p_y \end{pmatrix}, \quad (104)$$

where p_0 is the momentum of the reference particle.

Accordingly, we have from eq. 103

$$\frac{da}{ds} = h\zeta - \frac{Ze}{p_0} \left[\frac{dA_x}{ds} + \frac{\partial}{\partial x} \left(\frac{1}{\dot{s}} \varphi^C - \vec{A}^C \cdot \vec{v}^{C,s} \right) \right] \quad (105)$$

and

$$\frac{db}{ds} = -\frac{Ze}{p_0} \left[\frac{dA_y}{ds} + \frac{\partial}{\partial y} \left(\frac{1}{\dot{s}} \varphi^C - \vec{A}^C \cdot \vec{v}^{C,s} \right) \right]. \quad (106)$$

Expressing total derivative dA_x/ds in eq. 105 through partial derivatives as

$$\frac{dA_x}{ds} = \frac{\partial A_x}{\partial s} + \nabla A_x \cdot \vec{v}^{C,s} \quad (107)$$

and using the chain rule for $\partial A_x/\partial s$, we obtain

$$\frac{da}{ds} = h\zeta - \frac{Ze}{p_0} \left[\frac{1}{\dot{s}} \frac{\partial \varphi^C}{\partial x} + \frac{1}{\dot{s}} \frac{\partial A_x}{\partial t} - \frac{\partial}{\partial x} \left(\vec{A}^C \cdot \vec{v}^{C,s} \right) + \nabla A_x \cdot \vec{v}^{C,s} \right]. \quad (108)$$

Further, applying the expression

$$\vec{E} = -\nabla\varphi - \frac{\partial \vec{A}}{\partial t} \quad (109)$$

of the electric field \vec{E} through scalar potential φ and vector potential \vec{A} to eq. 108, we have

$$\begin{aligned} \frac{da}{ds} &= h\zeta + \frac{Ze}{p_0} \left[\frac{1}{\dot{s}} E_x + \frac{\partial}{\partial x} \left(\vec{A}^C \cdot \vec{v}^{C,s} \right) - \nabla A_x \cdot \vec{v}^{C,s} \right] = \\ &= h\zeta + \frac{Ze}{p_0} \left[\frac{1}{\dot{s}} E_x + \left(\vec{v}^{C,s} \times \left(\nabla \times \vec{A}^C \right) \right)_x \right]. \end{aligned} \quad (110)$$

This, considering the expression $\vec{B} = \nabla \times \vec{A}$ of magnetic field \vec{B} through vector potential \vec{A} , further simplifies to

$$\begin{aligned} \frac{da}{ds} &= h\zeta + \frac{Ze}{p_0} \left[\frac{1}{\dot{s}} E_x + \left(\vec{v}^{C,s} \times \vec{B}^C \right)_x \right] = \\ &= h\zeta + \frac{Ze}{p_0} \left[\frac{1}{\dot{s}} E_x + v_y^s B_s - v_s^s B_y \right]. \end{aligned} \quad (111)$$

But, as we found in eq. 91, $v_s^s = 1 + hx$, thus (compare with Berz, 1999)

$$\frac{da}{ds} = h\zeta + \frac{Ze}{p_0} \left[\frac{1}{\dot{s}} E_x + \frac{dy}{ds} B_s - (1 + hx) B_y \right]. \quad (112)$$

Similarly to the derivation of eq. 112 from eq. 105, we obtain from eq. 106 that

$$\frac{db}{ds} = \frac{Ze}{p_0} \left[\frac{1}{\dot{s}} E_y - \frac{dx}{ds} B_s + (1 + hx) B_x \right]. \quad (113)$$

Derivation of ODEs for positions For the kinematic momenta, considering eq. 102, we have

$$\frac{p_x}{p_s} = \frac{p_0 a}{p_s} = \left[(1 + hx) \frac{ds}{dx} \right]^{-1} \quad (114)$$

and

$$\frac{p_y}{p_s} = \frac{p_0 a}{p_s} = \left[(1 + hx) \frac{ds}{dy} \right]^{-1}, \quad (115)$$

from where we obtain (compare with Berz, 1999)

$$\frac{dx}{ds} = a(1 + hx) \frac{1}{\zeta} \quad (116)$$

and

$$\frac{dy}{ds} = b(1 + hx) \frac{1}{\zeta}. \quad (117)$$

Magnetic and electric rigidities The magnetic and electric rigidities are defined as

$$\chi_m = \frac{p}{Ze} \quad (118)$$

and

$$\chi_e = \frac{pv}{Ze}, \quad (119)$$

respectively, where p is the particle momentum, v its velocity, and Ze its charge. We note for the electric rigidity χ_{e0} of the reference particle that

$$\chi_{e0} = \frac{p_0 v_0}{Ze} = \frac{p_0^2}{\gamma_0 m Ze}. \quad (120)$$

Derivation of ODEs for scaled momenta (part 2) Inserting eq. 117 into eq. 112 and applying eq. 118, we have

$$\frac{da}{ds} = h\zeta + \frac{Ze}{p_0} \frac{1}{\bar{s}} E_x + \frac{B_s}{\chi_{m0}} b(1+hx) \frac{1}{\zeta} - \frac{B_y}{\chi_{m0}} (1+hx). \quad (121)$$

We now apply p_s from eq. 102 to eq. 121:

$$\frac{da}{ds} = h\zeta + (1+hx) \left(\frac{Ze}{p_0} m \frac{\gamma}{p_s} E_x + b \frac{1}{\zeta} \frac{B_s}{\chi_{m0}} - \frac{B_y}{\chi_{m0}} \right). \quad (122)$$

Further, we apply eqns. 120 and 104 to eq. 122, arriving at

$$\frac{da}{ds} = h\zeta + (1+hx) \left(\frac{\eta+1}{\eta_0+1} \frac{1}{\zeta} \frac{E_x}{\chi_{e0}} - \frac{B_y}{\chi_{m0}} + b \frac{1}{\zeta} \frac{B_s}{\chi_{m0}} \right), \quad (123)$$

where η is a relativistic measure defined as $\eta = \gamma - 1$.

Similarly to the derivations in eqns. 121–123 for da/ds , applying eqns. 116, 118, 120, and 102 to eq. 113 yields

$$\begin{aligned} \frac{db}{ds} &= \frac{Ze}{p_0} \frac{1}{\bar{s}} E_y - \frac{B_s}{\chi_{m0}} a(1+hx) \frac{1}{\zeta} + \frac{B_x}{\chi_{m0}} (1+hx) = \\ &= (1+hx) \left(\frac{Ze}{p_0} m \frac{\gamma}{p_s} E_y - a \frac{1}{\zeta} \frac{B_s}{\chi_{m0}} + \frac{B_x}{\chi_{m0}} \right) = \\ &= (1+hx) \left(\frac{\eta+1}{\eta_0+1} \frac{1}{\zeta} \frac{E_y}{\chi_{e0}} + \frac{B_x}{\chi_{m0}} - a \frac{1}{\zeta} \frac{B_s}{\chi_{m0}} \right). \end{aligned} \quad (124)$$

Derivation of an expression for ζ Inserting the expression $E = \gamma mc^2$ for relativistic energy E into the energy–momentum relation $E^2 = (pc)^2 + (mc^2)^2$, we obtain

$$\sqrt{\gamma^2 - 1} mc^2 = pc, \quad (125)$$

which we rewrite as

$$p = \sqrt{\eta(\eta+2)} mc. \quad (126)$$

Considering eq. 126, we express ζ in terms of a , b , and η as

$$\begin{aligned} \zeta &= \frac{p_s}{p_0} = \\ &= \sqrt{\frac{p^2}{p_0^2} - \frac{p_x^2}{p_0^2} - \frac{p_y^2}{p_0^2}} = \\ &= \sqrt{\frac{\eta(\eta+2)}{\eta_0(\eta_0+2)} - a^2 - b^2}. \end{aligned} \quad (127)$$

A.3.1 Result of the Derivation

The ODEs of motion of a charged particle in electromagnetic field are summarized from eqns. 116, 123, 117, and 124 as follows (compare with Makino and Berz, 2015):

$$\begin{aligned}
\frac{dx}{ds} &= a(1+hx) \frac{1}{\zeta}, \\
\frac{da}{ds} &= h\zeta + (1+hx) \left(\frac{\eta+1}{\eta_0+1} \frac{1}{\zeta} \frac{E_x}{\chi_{e0}} - \frac{B_y}{\chi_{m0}} + b \frac{1}{\zeta} \frac{B_s}{\chi_{m0}} \right), \\
\frac{dy}{ds} &= b(1+hx) \frac{1}{\zeta}, \\
\frac{db}{ds} &= (1+hx) \left(\frac{\eta+1}{\eta_0+1} \frac{1}{\zeta} \frac{E_y}{\chi_{e0}} + \frac{B_x}{\chi_{m0}} - a \frac{1}{\zeta} \frac{B_s}{\chi_{m0}} \right),
\end{aligned} \tag{128}$$

where E is the electrostatic field, B is the magnetic field, h is the reference orbit curvature, η is the relativistic measure $\eta = \gamma - 1$,

$$\chi_m = \frac{p}{Ze} \quad \text{and} \quad \chi_e = \frac{pv}{Ze} \tag{129}$$

are the magnetic and electric rigidities respectively,

$$\zeta = \frac{p_s}{p_0} = \sqrt{\frac{\eta(\eta+2)}{\eta_0(\eta_0+2)} - a^2 - b^2}, \tag{130}$$

and 0 refers to the reference particle.

In the non-relativistic limit $\eta \rightarrow 0$, the ODEs of motion from eq. 128 become

$$\begin{aligned}
\frac{dx}{ds} &= a(1+hx) \frac{1}{\zeta}, \\
\frac{da}{ds} &= h\zeta + (1+hx) \left(\frac{1}{\zeta} \frac{E_x}{\chi_{e0}} - \frac{B_y}{\chi_{m0}} + b \frac{1}{\zeta} \frac{B_s}{\chi_{m0}} \right), \\
\frac{dy}{ds} &= b(1+hx) \frac{1}{\zeta}, \\
\frac{db}{ds} &= (1+hx) \left(\frac{1}{\zeta} \frac{E_y}{\chi_{e0}} + \frac{B_x}{\chi_{m0}} - a \frac{1}{\zeta} \frac{B_s}{\chi_{m0}} \right),
\end{aligned} \tag{131}$$

where

$$\zeta = \frac{p_s}{p_0} = \sqrt{\frac{\eta}{\eta_0} - a^2 - b^2}. \tag{132}$$

B Inhomogeneity Coefficients of Electrostatic Spherical and Cylindrical Deflectors

According to Gauss' law, the radial component E_r of the electrostatic field of an electrostatic spherical deflector is

$$E_r(r) = \frac{Q}{4\pi\epsilon_0 r^2}, \tag{133}$$

where Q is the charge of the deflector's inner shell and r is the radius from the deflector's center of curvature. The tangential components of the electrostatic field are zero by spherical symmetry.

Similarly, by Gauss' law, the electrostatic field of a cylindrical deflector is subject to cylindrical symmetry, and its radial component E_r is

$$E_r(r) = \frac{\lambda}{2\pi\epsilon_0 r}, \tag{134}$$

where λ is the linear charge density of the deflector's inner shell.

The beamline coordinate x in both cases is $x = r - R_0$, where R_0 is the reference radius. Performing the Taylor series expansion of $E_x(x)$, we have

$$E_x(x) = \frac{Q}{4\pi\epsilon_0 R_0^2} \left(1 - 2\frac{x}{R_0} + 3\left(\frac{x}{R_0}\right)^2 \right) + O(x^3) \quad (135)$$

for the electrostatic spherical deflector and

$$E_x(x) = \frac{\lambda}{2\pi\epsilon_0 R_0} \left(1 - \frac{x}{R_0} + \left(\frac{x}{R_0}\right)^2 \right) + O(x^3) \quad (136)$$

for the electrostatic cylindrical deflector.

Comparing these results to the expansion

$$E(x) = E_0 \left[1 - \sum_{j=1}^N n_j \left(\frac{x}{R_0}\right)^j \right] + O(x^{N+1}) \quad (137)$$

from eq. 1, we obtain the inhomogeneity indices (n_1, n_2) as $(2, -3)$ for an electrostatic spherical deflector and $(1, -1)$ for an electrostatic cylindrical deflector.